Contrib Mineral Petrol (2017) 172:1
DOI 10.1007/s00410-016-1318-9

ORIGINAL PAPER

South-to-north pyroxenite–peridotite source variation correlated with an OIB-type to arc-type enrichment of magmas from the Payenia backarc of the Andean Southern Volcanic Zone (SVZ)

Frederik Ejvang Brandt[1] · Paul Martin Holm[1] · Nina Søager[1,2]

Received: 25 July 2016 / Accepted: 4 November 2016 / Published online: 5 December 2016

Abstract New high-precision minor element analysis of the most magnesian olivine cores ($Fo_{85–88}$) in fifteen high-MgO ($Mg\#_{66–74}$) alkali basalts or trachybasalts from the Quaternary backarc volcanic province, Payenia, of the Andean Southern Volcanic Zone in Argentina displays a clear north-to-south decrease in Mn/Fe_{ol}. This is interpreted as the transition from mainly peridotite-derived melts in the north to mainly pyroxenite-derived melts in the south. The peridotite–pyroxenite source variation correlates with a transition of rock compositions from arc-type to OIB-type trace element signatures, where samples from the central part of the province are intermediate. The southernmost rocks have, e.g., relatively low La/Nb, Th/Nb and Th/La ratios as well as high Nb/U, Ce/Pb, Ba/Th and Eu/Eu* = 1.08. The northern samples are characterized by the opposite and have Eu/Eu* down to 0.86. Several incompatible trace element ratios in the rocks correlate with Mn/Fe_{ol} and also reflect mixing of two geochemically distinct mantle sources. The peridotite melt end-member carries an arc signature that cannot solely be explained by fluid enrichment since these melts have relatively low Eu/Eu*, Ba/Th and high Th/La ratios, which suggest a component of upper continental crust (UCC) in the metasomatizing agent of the northern mantle. However, the addition to the mantle source of crustal materials or varying oxidation state cannot explain the variation in Mn and Mn/Fe of the melts and olivines along Payenia. Instead, the correlation between Mn/Fe_{ol} and whole-rock (wr) trace element compositions is evidence of two-component mixing of melts derived from peridotite mantle source enriched by slab fluids and UCC melts and a pyroxenite mantle source with an EM1-type trace element signature. Very low Ca/Fe ratios (~1.1) in the olivines of the peridotite melt component and lower calculated partition coefficients for Ca in olivine for these samples are suggested to be caused by higher H_2O contents in the magmas derived from subduction zone enriched mantle. Well-correlated Mn/Fe ratios in the wr and primitive olivines demonstrate that the Mn/Fe_{wr} of these basalts that only fractionated olivine and chromite reflects the Mn/Fe of the primitive melts and can be used as a proxy for the amount of pyroxenite melt in the magmas. Using Mn/Fe_{wr} for a large dataset of primitive Payenia rocks, we show that decreasing Mn/Fe_{wr} is correlated with decreasing Mn and increasing Zn/Mn as expected for pyroxenite melts.

Keywords Andean Southern Volcanic Zone · Backarc · Primitive basalts · Olivine · Pyroxenite · Mn/Fe · Upper continental crust

Communicated by Timothy L. Grove.

Electronic supplementary material The online version of this article (doi:10.1007/s00410-016-1318-9) contains supplementary material, which is available to authorized users.

✉ Frederik Ejvang Brandt
feb@ign.ku.dk

[1] Department of Geoscience and Natural Resource Management, University of Copenhagen, Øster Voldgade 10, 1350 Copenhagen K, Denmark

[2] Geomar Helmholtz Centre for Ocean Research Kiel, Wischhofstraβe1-3, 24148 Kiel, Germany

Introduction

Variability of mantle melts, as recognized in terms of isotopic, major or trace element variations in Ocean Island Basalts (OIB), supports the involvement of recycled oceanic and/or continental crustal components in their mantle

sources (e.g., Hofmann and White 1982; Stracke et al. 2005; Willbold and Stracke 2006; Jackson et al. 2007; Sobolev et al. 2005, 2007; Jackson and Dasgupta 2008). Oceanic lithosphere including crust and sediments enters the mantle at subduction zones and is modified through mineral dehydration reactions and melting that metasomatizes the overlying mantle wedge or causes mantle wedge melting (e.g., Grove et al. 2006). Also upper or lower continental crust or lithospheric mantle may be abraded from the continent by subduction erosion (e.g., Scholl et al. 1980; von Huene and Scholl 1991; Stern 1991, 2011; Kay et al. 2005; Holm et al. 2014) or enter the mantle by delamination processes (e.g., Kay and Kay 1993; Lee et al. 2006). These processes recycle crust into the mantle where it recrystallizes to pyroxenite and sinks deeper into the mantle. The pyroxenite may later be entrained in mantle upwellings and contribute to, for example, OIB magmas (e.g., Hofmann and White 1982; Sobolev et al. 2005, 2007; Herzberg 2006, 2011). Sobolev et al. (2005, 2007) suggest that siliceous melts of recycled crust (as eclogite) in plumes react with the ambient solid peridotite to produce olivine-free pyroxenites which subsequently melt and contribute to OIB. Similarly, the release of siliceous components from the subduction channel will diversify the mantle wedge composition and potentially change its mineralogy by converting mantle olivine to pyroxenes (e.g., Straub et al. 2008, 2011, 2014).

To discriminate between peridotite and pyroxenite melts, Sobolev et al. (2007) suggested using the ratios Mn/Fe, Ca/Fe and Ni/(Mg/Fe) in olivines. These elements are used because of their compatible nature in either olivine or pyroxene, and the concentration of the elements in the melt is controlled by the residual amount of these minerals in the source rock (Sobolev et al. 2005, 2007; Le Roux et al. 2011; Herzberg 2011). Olivine is the first mineral to crystallize in magmas cooling in the crust and will record the geochemical variation in mantle melts caused by differences in the source mineralogy. Olivine fractionation lowers Ni/(Mg/Fe), and later fractionation of other minerals than olivine will change the Mn/Fe and Ca/Fe ratios. Therefore, highly fosteritic olivines from the most primitive melts are needed. Moreover, Le Roux et al. (2010, 2011) suggested using ratios of transition elements in whole rocks such as Zn/Fe and Zn/Mn with contrasting compatibilities in olivine and pyroxenes to trace pyroxenite in the source of mantle melts. We will apply these two approaches on basalts from the Payenia province in order to investigate the role of recycled crustal components in their mantle sources.

Due to scarcity of undifferentiated magmas in the arc volcanoes of the Andean Southern Volcanic Zone (SVZ), the acquisition of mantle melt geochemical signatures is challenging. By contrast, in the Payenia backarc province of the SVZ, rocks with primitive basaltic compositions are widespread. We use whole-rock major and trace element analyses and high-precision olivine analyses in a selection of the most primitive samples to obtain information on source mineralogy between a typical EM1-type component in southern Payenia and a subduction-modified component in northern Payenia (Kay et al. 2006a, 2013; Jacques et al. 2013; Søager and Holm 2013; Søager et al. 2013, 2015a). We show that the mantle sources are extremely different in terms of mineralogy and trace element chemistry. The bulk rock trace element chemistry of the most primitive Payenia basalts is directly coupled to variations in their mantle source lithology. We argue that the arc signature of the northern backarc magmas is preserved in a peridotitic mantle source, whereas the most southern magmas mainly originate from pyroxenite melting as also proposed by Søager and Holm (2013) and Søager et al. (2015b). We discuss the use of Mn/Fe, Ca/Fe and various transition metal ratios for identification of pyroxenite- and peridotite-derived melts in the Payenia rocks and olivines. We consider the effects of varying oxidation state of the primary melts, H_2O contents and the addition to the mantle source of subducted crustal materials. We argue that these effects are of less importance to the major and minor element compositions of melts in Payenia than the relative roles of peridotite and pyroxenite.

Geological setting

The Payenia backarc province (Fig. 1) of the Andean Southern Volcanic Zone (SVZ) arc at 33.3°S–37.3°S covers an area of 40,000 km^2 with over 800 mono- and small polygenetic volcanoes and a few larger volcanic complexes such as the Payún Matrú and Cerro Nevado composite volcanoes (e.g., Ramos and Folguera 2011). The Quaternary volcanism in Payenia occurred in seven volcanic fields (VF): Payún Matrú, Río Colorado, Auca Mahuida and Tromen in the south, and Llancanelo, Nevado and the Northern Segment in the north (Fig. 1). The Payenia province is situated in the backarc of the NSVZ (33–34.4°S), the TSVZ (34.4–36.1°S) and the CSVZ (south of 36.1°S) according to the division of Holm et al. (2014). In the area north of Payenia and the SVZ, called the Pampean (Chilean) flat-slab segment at 26°S–33°S, there is no Quaternary volcanism. The termination of volcanism here has been coupled to the subduction of the Juan Fernandez ridge (Kay and Mpodozis 2002). Seismicity around 33°S indicates an abrupt transition from a 30° slab dip under the TSVZ to a horizontal slab dip under the Pampean flat-slab segment (Cahill and Isacks 1992) with NSVZ and the Northern Segment of Payenia overlying this transition. The Payenia province experienced a period of shallow slab subduction in Mid-Miocene to Early Pleistocene times with an eastward

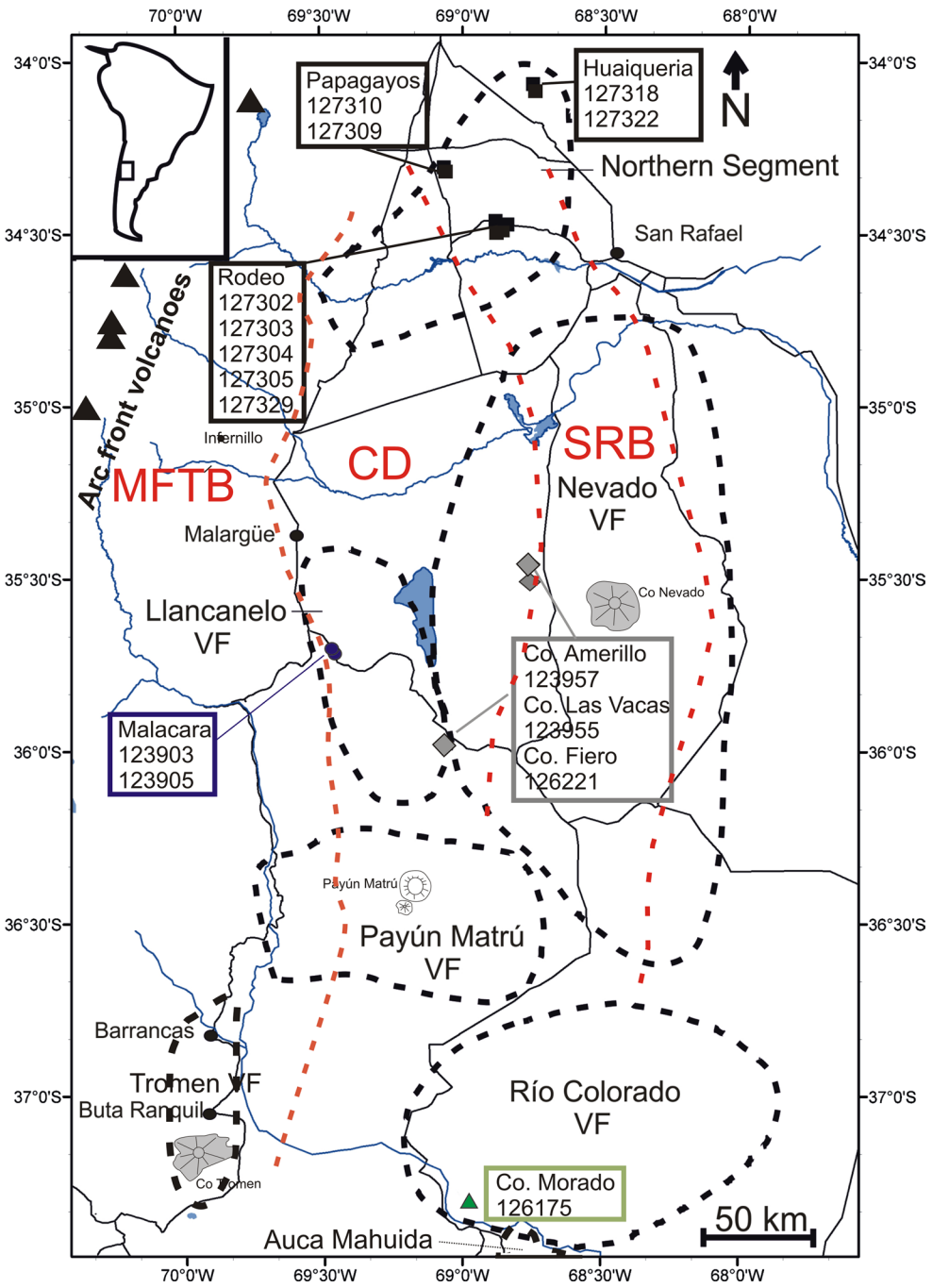

Fig. 1 Map of the Payenia volcanic backarc province east of the volcanic frontal arc of the Andean Southern Volcanic Zone with volcanic fields (VF) according to Gudnason et al. (2012): Northern Segment VF, Nevado VF, Llancanelo VF, Payún Matrú VF, Río Colorado VF, Auca Mahuida VF and Tromen VF. Sample locations: Northern Segment—*black squares*, Llancanelo—*blue circles*, Nevado—*gray diamonds* and Río Colorado—*green triangle*. *Red stippled lines* delimit major tectonic features. From west to east, Marlargüe fold and trust belt (MFTB), the Central Depression (CD) and the San Rafael Block (SRB)

broadening of the arc extending to the San Rafael block (SRB, Fig. 1) (Kay et al. 2004, 2006a, b; Kay and Copeland 2006; Dyhr et al. 2013a, b; Litvak et al. 2015). The SRB is a basement block uplifted during the compressional tectonic regime in the Miocene shallow slab period (Ramos and Kay 2006; Folguera et al. 2009). It underlies the main part of the Nevado and Northern Segment. The Early Pleistocene OIB-like volcanism of Auca Mahuida and Río Colorado marks the end of the shallow subduction in this area, while alkaline slab modified basalts erupted in the Nevado volcanic field at this time (Bertotto et al. 2009; Kay et al. 2006a, 2013; Jacques et al. 2013; Søager et al. 2013). Volcanism shifted west to Payún Matrú, Llancanelo and the Northern Segment at ~0.5 Ma, suggesting roll back of the subducting Nazca plate (Folguera et al. 2009; Gudnason et al. 2012).

Previous work

Nd, Sr, Hf and Pb isotopes suggest that distinct mantle sources are needed to explain the northern and southern Payenia volcanism (Jacques et al. 2013; Søager et al. 2015a). The isotopic signatures of the northern backarc basalts overlap with those of the SVZ arc rocks. In Sr–Nd–Hf isotopic space, the SVZ arc overlaps the field of South Atlantic MORB mantle (Jacques et al. 2013; Søager et al. 2015a). In contrast, the Quaternary magmas of southern Payenia have less radiogenic Pb, Sr and Hf at a given Nd than the northern backarc magmas and the SVZ arc (Jacques et al. 2013; Søager et al. 2015a). The SVZ arc and backarc magmas are isotopically distinct from Pacific MORB, precluding influence on the magmas by melts derived from the subducting slab (Holm et al. 2014; Søager et al. 2015a). High field strength element (HFSE) ratios indicate a highly depleted mantle beneath the SVZ arc, but a less depleted pre-metasomatic mantle beneath northern Payenia (Søager et al. 2015a). The southern backarc mantle source has an EM1-type trace element signature (Jacques et al. 2013; Kay et al. 2013; Søager et al. 2013, 2015a; Søager and Holm 2013).

Kay et al. (2013) suggested that the trace element and isotope characteristics of the Auca Mahuida and Río Colorado magmas indicate melting of asthenosphere with delaminated components of metasomatized subcontinental lithosphere (including lower continental crust). Based on Hf isotopes, Jacques et al. (2013) similarly proposed that both the depleted and enriched mantle of Payenia lie within differently enriched parts of South American Proterozoic subcontinental lithosphere. In contrast, Søager and Holm (2013) suggested that the EM1 source is recycled oceanic and lower continental crust upwelling beneath the southern Payenia region. In an olivine study of southern Payenia basalts mainly from Río Colorado, Søager et al. (2015b) showed that these magmas approximate pure pyroxenite melts and magmatic temperature estimates suggested they were asthenospheric melts. However, the Río Colorado basalts were found to fall in a high- and a low-Nb/U group with distinct major and trace element compositions but entirely overlapping isotopic compositions, and the high K_2O contents and lower indicated magmatic temperatures of the low-Nb/U basalts led Søager et al. (2015b) to interpret these as lithospheric mantle melts. The Río Colorado sample 126175 used in this study falls in this group of low-Nb/U basalts.

Rock samples

This study focuses on the north-to-south compositional variation in Payenia with an emphasis on the northern part. The Northern Segment (Fig. 1) volcanism constitutes several groups or small isolated monogenetic volcanic centers and one larger stratovolcano, Cerro Diamante (Folguera et al. 2009; Ramos and Folguera 2011) with ages ranging from 0.06 to 0.7 Ma (Folguera et al. 2009; Gudnason et al. 2012). This study includes nine samples from the Northern Segment from the volcano groups Huaiqueria, Papagayos, Rodeo and Loma del Medio (Fig. 1; Table 1). Three samples are from the 0.8–2.8 Ma Nevado volcanic field (Quidelleur et al. 2009; Gudnason et al. 2012) consisting of numerous volcanic cones, lava flows, smaller volcanoes and the big Cerro Nevado volcano. Two samples are from the Llancanelo volcanic field composed of several monogenetic volcanic centers of cinder cones and small lava flows. The last sample comes from the Río Colorado volcanic

Table 1 Sample names and locations

Sample ID	Volcanic field	Group	Volcano	Latitude	Longitude
127318	Northern Segment	Huaiqueria	Huiaqueria	−34.0697	−68.7543
127322	Northern Segment	Huaiqueria	Huiaqueria	−34.0789	−68.7271
127310	Northern Segment	Papagayos	Co. Guadaloso	−34.3110	−69.0652
127309	Northern Segment	Papagayos	near Co Guadaloso	−34.3092	−69.0737
127305	Northern Segment	Medio	Co Ao Hondo	−34.4952	−69.2327
127304	Northern Segment	Rodeo	Co. Chico.	−34.4677	−68.8842
127302	Northern Segment	Rodeo	East of Co. del Medio	−34.4779	−68.8423
127303	Northern Segment	Rodeo	East of Co. del Medio	−34.4779	−68.8423
127329	Northern Segment	Rodeo	Co. del Medio	−34.4825	−68.8726
123957	Nevado		Co. Las. Vagas	−35.4659	−68.7778
123955	Nevado		Co. Amerillo	−35.5141	−68.7614
123903	Llancanelo		Malacara	−35.7094	−69.4631
123905	Llancanelo		Malacara	−35.7219	−69.4538
126221	Llancanelo		Co. Fiero	−35.9883	−69.0643
126175	Río Colorado		Co. Morado	−37.3042	−69.0184

field in the southern part of Payenia and is represented by sample 126175 from the 1.0 Ma Co. Morado volcano (Gudnason et al. 2012; Søager et al. 2013). Whole-rock analyses of the samples from Nevado, Llancanelo and Río Colorado were published in Søager et al. (2013).

Petrography

All samples are basaltic with around 5–15% olivine phenocrysts, 0.5–3 mm in size. Additionally, 1–6% clinopyroxene phenocrysts are found in samples from the Northern Segment, whereas sparse plagioclase phenocrysts (1%) are only observed in Rodeo samples 127303 and 127329. Samples from Llancanelo, Nevado and Río Colorado contain olivine phenocrysts only. The olivine phenocrysts are optically homogenous in composition. All lavas and olivine phenocrysts in particular appear fresh with no signs of alteration.

Analytical methods

At least ten olivine phenocryst cores of each sample were initially analyzed under routine analytical conditions on a JEOL JXA 8200 electron microprobe at the Department of Geosciences and Natural Resource Management, University of Copenhagen. For each sample, the most forsteritic cores were selected for high-precision analysis and only olivines with $Fo^{\#}$ >85 (where $Fo^{\#} = Mg/(Mg + Fe)$ mol/mol) were considered for publication to avoid any potential effects on olivine chemistry by magmatic differentiation processes in the crust. More specifically, we have tried to avoid olivines that have crystallized from contaminated melts as well as melts that have experienced clinopyroxene fractionation. We present 51 high-precision analyses in total from 15 samples where 1–7 olivine cores were analyzed in each. For high-precision analysis, the microprobe setup was 15 kV accelerating voltage, 70 nA electron current, peak counting times of 120 s for Ni, Mn and Ca and background counting times of mostly 60 s for each point constituting an analysis. Counting times for all elements are given in Supplementary material 1. Each reported result represents 6–7 closely spaced (within an area of 10 µm) spot analyses in the olivine core, and this resulted in a 6*120 s = 720 s peak and 6*60 s = 360 s background measurement time for each analysis (Mn, Ca and Ni). This allowed detection of inhomogeneity due to impurities or imperfect state of the mineral and thus exclusion of such spot analysis and improved the analytical precision (Supplementary material 1). Detection limits were below 20, 2 and 7 ppm for Ni, Ca and Mn, respectively, categorizing them as precision to high-precision analyses according to Sobolev et al. (2007). Precision of the olivine core analyses is reported at the 95% confidence level in Table 2 for the concentrations and in Table 3 for the various derived ratios. Calibration was done on natural and synthetic standards, and the current was monitored throughout the analytical session to ensure internal consistency of the data. Two reproducibility test runs ($N = 40$ and 51) of the Marjalahti olivine standard gave $SiO_2 = 39.53 \pm 0.70$ and 40.63 ± 0.27 (2σ), $MgO = 47.78 \pm 0.37$ and 47.50 ± 0.43 (2σ), $FeO = 11.37 \pm 0.21$ and 11.06 ± 0.18 (2σ), $Fo^{\#} = 88.22 \pm 0.16$ and 88.45 ± 0.17 (2σ), and $MnO = 0.301 \pm 0.013$ and 0.303 ± 0.010 (2σ), respectively, and are presented in Supplementary material 2. This standard has very low Ni, Cr and CaO. Four olivines have very low Ca and Cr contents and are considered xenocrystic of origin (e.g., Foley et al. 2013). These xenocrysts are not addressed further, but are listed in Supplementary material 3 along with all the olivine analysis.

For whole-rock analysis, nine samples from the Northern Segment, petrographically judged to be unaltered, were jaw crushed and subsequently powdered in an agate mill. Major elements were analyzed at the Acme Analytical Laboratories Ltd., Canada (Acme Labs; Code 4A), by fusion of the samples into glass and analysis by ICP-AES. Volatile contents were estimated by loss on ignition at 1000 °C. After dissolution of the samples, ICP-MS analysis was carried out on a PerkinElmer 6100 DRC Quadrupole at GEUS (Geological Survey of Denmark and Greenland). The data are presented in Table 4. Reproducibility of international standards BHVO-2 and BCR-2 in the period of analyses is 3–4 rel.% (2σ, $n = 45$) for most elements. Results for all incompatible elements discussed in this paper deviate less from the GeoReM preferred values (Jochum and Nehring 2006) than the 2σ uncertainty. For details of methods and results, see Supplementary material 4.

Results

Olivine compositions

High-precision analyses of olivine cores range between Fo_{85} and Fo_{89}. Mn contents range from 1200 to 1800 ppm (Fig. 2a; Table 2). Olivine cores from Río Colorado sample 126175 (low-Nb/U group of Søager and Holm 2013) have the lowest Mn contents at a given $Fo^{\#}$. Olivines from the Northern Segment have the highest Mn contents, and olivines from Nevado and Llancanelo are intermediate. The Ni contents range from 1400 to 2800 ppm and decrease with $Fo^{\#}$ (Fig. 2b). There is no significant Ni variation along Payenia at a given $Fo^{\#}$. The Ca content is relatively low and varies from 1000 to 1600 ppm (Fig. 2c). Olivines from Río Colorado have the highest Ca contents, whereas olivines

Table 2 High-precision major and minor elements in olivine

Area	Sample ID	Fo#	2σ	2σ (rel%)	Mg (wt%)	2σ (wt%)	2σ (rel%)	Fe (wt%)	2σ (wt%)	2σ (rel%)	Ni (ppm)	2σ (ppm)	2σ (rel%)
Northern Segment													
	Huaiqueria												
	127318_5	85.58	0.16	0.2	27.79	0.26	0.9	10.76	0.06	0.6	1676	46	2.7
	127318_9	85.63	0.29	0.3	28.45	0.57	2.0	10.97	0.06	0.5	1497	26	1.7
	127322_10	86.27	0.09	0.1	27.85	0.09	0.3	10.19	0.08	0.8	1716	58	3.4
	127322_3	87.13	0.04	0.0	28.29	0.03	0.1	9.60	0.04	0.4	2195	75	3.4
	Papagayos												
	127310_4	88.11	0.11	0.1	29.15	0.08	0.3	9.04	0.09	1.0	2436	14	0.6
	127310_7	86.63	0.06	0.1	28.54	0.05	0.2	10.12	0.05	0.5	1653	38	2.3
	127310_3	87.03	0.08	0.1	28.66	0.08	0.3	9.81	0.07	0.7	1788	20	1.1
	127309_1	87.78	0.10	0.1	28.33	0.14	0.5	9.06	0.09	1.0	1967	76	3.9
	127309_4	88.31	0.07	0.1	28.41	0.19	0.7	8.64	0.07	0.8	2611	81	3.1
	127309_5	87.22	0.08	0.1	28.11	0.10	0.3	9.46	0.04	0.5	1734	83	4.8
	127309_8	88.60	0.04	0.1	28.88	0.05	0.2	8.53	0.04	0.5	2406	72	3.0
	Loma del Medio												
	127305_1	87.68	0.04	0.1	28.37	0.07	0.3	9.16	0.03	0.3	2182	64	2.9
	127305_10	87.99	0.10	0.1	28.51	0.15	0.5	8.94	0.07	0.7	2062	132	6.4
	127305_6	87.52	0.13	0.2	28.01	0.07	0.2	9.17	0.09	1.0	1978	33	1.7
	127305_7	87.65	0.06	0.1	28.25	0.03	0.1	9.15	0.05	0.5	2339	68	2.9
	Rodeo												
	127304_6	87.75	0.07	0.1	29.00	0.08	0.3	9.30	0.05	0.5	2828	44	1.6
	127304_9	88.33	0.05	0.1	28.90	0.04	0.1	8.78	0.05	0.5	2796	30	1.1
	127302_3	85.65	0.12	0.1	27.71	0.05	0.2	10.67	0.09	0.9	2051	22	1.1
	127302_2	86.15	0.28	0.3	27.29	0.15	0.5	10.08	0.19	1.9	2473	46	1.8
	127302_6	86.02	0.14	0.2	27.57	0.07	0.2	10.29	0.10	1.0	2206	46	2.1
	127302_11	86.48	0.07	0.1	27.75	0.07	0.2	9.97	0.05	0.5	2104	71	3.4
	127302_8	86.42	0.10	0.1	27.72	0.07	0.3	10.01	0.07	0.7	2199	65	3.0
	127303_10	86.19	0.08	0.1	28.06	0.05	0.2	10.33	0.06	0.6	2293	32	1.4
	127329_2	87.01	0.04	0.0	28.43	0.05	0.2	9.75	0.05	0.5	1768	46	2.6
	127329_5	87.31	0.05	0.1	28.49	0.07	0.2	9.52	0.05	0.5	2118	28	1.3
	127329_8	85.28	0.03	0.0	27.84	0.03	0.1	11.04	0.03	0.2	1384	14	1.0
Nevado													
	123957_1	85.91	0.06	0.1	27.94	0.07	0.2	10.53	0.05	0.5	1506	34	2.2
	123955_1	87.15	0.03	0.0	28.30	0.02	0.1	9.59	0.03	0.4	2712	22	0.8
	123955_3	86.66	0.03	0.0	28.12	0.03	0.1	9.94	0.02	0.2	2263	40	1.7

Table 2 continued

Area	Sample ID	Fo#	2σ	2σ (rel%)	Mg (wt%)	2σ (wt%)	2σ (rel%)	Fe (wt%)	2σ (wt%)	2σ (rel%)	Ni (ppm)	2σ (ppm)	2σ (rel%)
	123955_8	85.76	0.06	0.1	27.75	0.05	0.2	10.58	0.05	0.5	2071	48	2.3
	123955_9	86.53	0.09	0.1	27.96	0.05	0.2	10.00	0.07	0.7	2631	78	3.0
	126221_2a	87.30	0.07	0.1	28.58	0.04	0.1	9.55	0.05	0.6	2370	30	1.3
	126221_3	86.22	0.05	0.1	27.99	0.03	0.1	10.28	0.05	0.4	1673	44	2.6
	126221_8	86.13	0.04	0.0	27.99	0.05	0.2	10.36	0.04	0.4	1883	14	0.7
	126221_2b	88.70	0.03	0.0	30.06	0.03	0.1	9.35	0.03	0.4	2317	36	1.6
	126221_10	87.12	0.07	0.1	28.86	0.03	0.1	9.80	0.06	0.6	2127	30	1.4
Llancanelo													
	123903_10	85.63	0.30	0.4	27.55	0.12	0.4	10.62	0.21	2.0	1681	102	6.1
	123903_2	87.11	0.05	0.1	28.03	0.06	0.2	9.53	0.05	0.5	2304	58	2.5
	123903_3	85.77	0.07	0.1	27.78	0.04	0.1	10.58	0.06	0.6	1683	69	4.1
	123903_8	86.28	0.11	0.1	27.86	0.04	0.1	10.18	0.10	1.0	2054	29	1.4
	123903_9	87.07	0.14	0.2	28.00	0.08	0.3	9.56	0.10	1.0	2491	25	1.0
	123905_1	87.69	0.03	0.0	28.85	0.10	0.3	9.30	0.04	0.4	2479	30	1.2
	123905_2	86.92	0.08	0.1	28.62	0.11	0.4	9.89	0.05	0.5	2554	22	0.9
Río Colorado													
	126175_8a	85.69	0.09	0.1	27.47	0.07	0.2	10.54	0.07	0.7	1813	40	2.2
	126175_8b	85.65	0.07	0.1	27.40	0.03	0.1	10.54	0.06	0.6	1806	32	1.8
	126175_9a	86.51	0.46	0.5	27.70	0.14	0.5	9.93	0.34	3.5	2164	226	10.4
	126175_9b	86.57	0.06	0.1	27.70	0.03	0.1	9.89	0.06	0.6	2227	20	0.9
	126175_9c	86.31	0.14	0.2	27.59	0.07	0.2	10.06	0.12	1.2	2236	74	3.3
	126175_10a	86.37	0.04	0.0	27.54	0.06	0.2	9.99	0.05	0.5	2341	34	1.5
	126175_10b	86.38	0.06	0.1	27.70	0.04	0.1	10.03	0.06	0.6	2351	40	1.7
Average 2σ			0.09			0.08			0.07			50	

Area	Sample ID	Mn (ppm)	2σ (ppm)	2σ (rel%)	Ca (ppm)	2σ (ppm)	2σ (rel%)	Cr (ppm)	2σ (ppm)	2σ (rel%)
Northern Segment										
	Huaiqueria									
	127318_5	1792	49	2.7	1143	24	2.1	135	56	41
	127318_9	1762	15	0.9	1203	42	3.5	117	50	43
	127322_10	1633	27	1.7	1130	18	1.6	153	17	11
	127322_3	1489	20	1.3	1053	23	2.2	185	23	12
	Papagayos									
	127310_4	1321	31	2.3	994	16	1.6	567	82	14
	127310_7	1507	18	1.2	1088	14	11.2	186	42	23
	127310_3	1469	19	1.3	1120	14	1.3	168	30	18

Table 2 continued

Area	Sample ID	Mn (ppm)	2σ (ppm)	2σ (rel%)	Ca (ppm)	2σ (ppm)	2σ (rel%)	Cr (ppm)	2σ (ppm)	2σ (rel%)
	127309_1	1361	14	1.0	1098	32	2.9	233	30	13
	127309_4	1256	30	2.4	1018	92	9.0	340	36	11
	127309_5	1405	32	2.2	1130	25	2.2	169	46	27
	127309_8	1295	23	1.8	1019	20	1.9	272	56	19
	Loma del Medio									
	127305_1	1436	15	1.1	1079	18	1.6	177	15	8
	127305_10	1349	19	1.4	1191	97	8.2	160	26	17
	127305_6	1426	16	1.1	1091	17	1.5	173	17	10
	127305_7	1416	15	1.0	997	5	0.5	161	34	21
	Rodeo									
	127304_6	1335	30	2.2	1189	42	3.5	240	38	16
	127304_9	1328	13	1.0	1027	16	1.6	269	26	10
	127302_3	1701	37	2.1	1056	13	1.2	110	38	34
	127302_2	1740	71	4.1	1391	41	2.9	307	85	28
	127302_6	1637	20	1.2	1120	49	4.4	155	23	15
	127302_11	1462	29	2.0	1227	12	1.0	141	16	11
	127302_8	1660	55	3.3	1149	20	1.7	130	23	18
	127303_10	1727	34	2.0	1135	20	1.7	201	20	10
	127329_2	1474	12	0.8	1116	12	1.1	115	32	28
	127329_5	1410	34	2.4	1114	7	0.6	208	56	27
	127329_8	1731	25	1.4	1240	12	1.0	95	20	21
Nevado										
	123957_1	1607	52	3.2	1377	40	2.9	191	18	9
	123955_1	1356	16	1.1	1137	4	0.3	453	53	12
	123955_3	1473	22	1.5	1270	22	1.7	190	21	11
	123955_8	1550	16	1.0	1316	9	0.7	188	23	12
	123955_9	1438	36	2.4	1105	29	2.6	387	48	12
	126221_2a	1404	15	1.1	1033	12	1.2	242	30	12
	126221_3	1591	22	1.4	1193	16	1.3	229	34	15
	126221_8	1589	18	1.1	1174	11	0.9	183	32	18
	126221_2b	1363	31	2.3	1135	34	3.0	463	69	15
	126221_10	1403	27	1.9	1145	38	3.3	266	63	24
Llancanelo										
	123903_10	1542	47	3.0	1290	30	2.3	207	50	24
	123903_2	1342	19	1.4	1293	23	1.8	255	17	7
	123903_3	1511	20	1.2	1419	14	1.0	176	23	13

Table 2 continued

Area	Sample ID	Mn (ppm)	2σ (ppm)	2σ (rel%)	Ca (ppm)	2σ (ppm)	2σ (rel%)	Cr (ppm)	2σ (ppm)	2σ (rel%)
	123903_8	1440	17	1.2	1315	26	2.0	277	31	11
	123903_9	1315	16	1.2	1227	28	2.3	340	30	9
	123905_1	1264	22	1.7	1241	16	1.3	340	22	6
	123905_2	1321	34	2.6	1305	26	2.0	373	58	16
Río Colorado										
	126175_8a	1407	31	2.2	1588	28	1.8	323	32	10
	126175_8b	1433	29	2.0	1648	24	1.5	244	46	19
	126175_9a	1281	50	3.9	1474	114	7.7	280	40	14
	126175_9b	1294	16	1.2	1418	8	0.6	375	48	13
	126175_9c	1357	51	3.8	1513	60	4.0	305	36	12
	126175_10a	1287	32	2.5	1294	10	0.8	276	24	9
	126175_10b	1269	19	1.5	1301	18	1.4	349	44	13
Average 2σ			27			27			36	

2σ = standard error of the mean (SEM)*2

from Llancanelo, the Northern Segment and Nevado have similar and lower Ca contents. The Cr concentration ranges from 100 to 600 ppm and overall increases from north to south at a given $Fo^{\#}$ (Fig. 2d).

Olivines show no correlation between $Fo^{\#}$ and olivine Mn/Fe ($r^2 = 0.05$) (Fig. 3a). The lowest Mn/Fe_{ol} ratios are from Río Colorado (126175) which have an average for seven olivines of 100Mn/Fe = 1.31 (Table 3) similar to other olivines from Río Colorado (Søager et al. 2015b). This places the Río Colorado olivines in the very end of the global olivine array (Sobolev et al. 2007; Fig. 3c, d), indicating that they are close to pure pyroxenite melts. There is an overall south-to-north increase in Mn/Fe_{ol} (Fig. 3b), and the highest Mn/Fe_{ol} ratios are found in olivines from the Northern Segment extending to values typical for olivines crystallizing from peridotite melts (Fig. 3c, d). However, the Ca/Fe ratios in the Northern Segment and Nevado olivines are as low as in the Río Colorado olivines and much lower than Ca/Fe in olivines crystallizing from peridotite-derived melts as reported by Sobolev et al. (2007). Therefore, the 100Ca/Fe versus 100Mn/Fe trend (Fig. 3d) differs strongly from the MORB-OIB array and defines a negatively correlated trend toward lower Ca/Fe in the high-Mn/Fe peridotite end-member. Payenia olivine ratios of Ni/(Mg/Fe)/1000 (Fig. 3c) overlap the peridotite end of the MORB-OIB array defined by Sobolev et al. (2007) at high 100Mn/Fe, but fall below the pyroxenite end at low 100Mn/Fe, although the samples from Søager et al. (2015b) with lowest 100Mn/Fe do have elevated Ni/(Mg/Fe)/1000 relative to the other Payenia olivines. This was explained by Søager et al. (2015b) as due to small amounts of olivine fractionation which lowers Ni/(Mg/Fe)/1000 at these Fo contents.

Rock compositions

The host rocks (Table 4) are primitive alkali basalts or trachybasalts with MgO ranging from 10.0 to 14.6 wt%, SiO_2 contents from 45 to 48 wt%, and Mg# = 66–74. Most samples have CaO contents within the range 9 to 11 wt%, but sample 126175 from Río Colorado has 7.2 wt% CaO (Fig. 4a).

The Northern Segment samples from Huaiqueria, Papagayos and the Rodeo Group have characteristic arc-type trace element patterns with enrichments in LREE (light rare earth elements), Th and fluid-mobile LIL (large ion lithophile) elements (e.g., Rb, Ba, Sr and Pb) along with depletions in fluid-immobile HFS (high field strength) elements (Nb, Ta and Ti) (Fig. 4b). The arc signature decreases southward to the OIB-type trace element signature characteristic of samples from Río Colorado (Søager et al. 2013, Jacques et al. 2013; Kay et al. 2013) with no negative Nb or Ta anomaly. The southernmost sample at Río Colorado

Table 3 High-precision major and minor elements ratios in olivine

Volc. field	Sample ID	100 Mn/Fe	2σ[1]	2σ (%)	Ni/(Mg/Fe)/1000	2σ	2σ (%)	100Ca/Fe	2σ	2σ (%)	Xpx (%)	2σ	Xpx avg (%)	100Mn/Fe avg	100Ca/Fe avg	S Latitude
Northern segment																
	Huaiqueria															
	127318_5	1.665	0.038	2.3	0.649	0.014	2.2	1.062	0.025	2.4	3.2	7.9	9.3	1.636	1.079	34.1
	127318_9	1.606	0.012	0.7	0.577	0.015	2.6	1.096	0.041	3.7	15.4	2.5				
	127322_10	1.604	0.020	1.2	0.627	0.020	3.2	1.110	0.022	2.0	15.9	4.1	21.3	1.577	1.104	34.1
	127322_3	1.551	0.020	1.3	0.745	0.026	3.5	1.097	0.026	2.3	26.8	4.1				
Papagayos																
	127310_4	1.462	0.039	2.7	0.755	0.008	1.1	1.100	0.013	1.2	45.2	8.1	40.9	1.482	1.105	34.3
	127310_7	1.488	0.014	0.9	0.586	0.012	2.0	1.075	0.017	1.6	39.8	2.9				
	127310_3	1.497	0.018	1.2	0.612	0.008	1.3	1.141	0.014	1.2	38.0	3.7				
	127309_1	1.502	0.013	0.9	0.629	0.019	3.1	1.212	0.030	2.5	36.8	2.8	39.5	1.490	1.195	34.3
	127309_4	1.453	0.037	2.5	0.794	0.021	2.6	1.178	0.104	8.8	47.0	7.7				
	127309_5	1.484	0.033	2.2	0.584	0.025	4.3	1.193	0.024	2.0	40.7	6.8				
	127309_8	1.519	0.026	1.7	0.710	0.021	3.0	1.195	0.025	2.1	33.4	5.4				
Loma del Medio																
	127305_1	1.568	0.019	1.2	0.704	0.018	2.6	1.179	0.018	1.5	23.2	3.8	28.0	1.545	1.198	34.5
	127305_10	1.510	0.028	1.9	0.646	0.042	6.5	1.333	0.113	8.5	35.3	5.5				
	127305_6	1.555	0.015	1.0	0.648	0.008	1.2	1.189	0.013	1.1	26.0	3.2				
	127305_7	1.548	0.013	0.8	0.757	0.023	3.0	1.090	0.010	0.9	27.4	2.7				
Rodeo																
	127304_6	1.435	0.028	2.0	0.907	0.014	1.5	1.278	0.045	3.5	50.9	5.8	42.7	1.474	1.224	34.5
	127304_9	1.514	0.014	0.9	0.849	0.012	1.4	1.17	0.017	1.5	34.5	2.9				
	127302_3	1.594	0.029	1.8	0.789	0.012	1.5	0.99	0.018	1.8	17.9	6.0	17.6	1.607	1.156	34.5
	127302_2	1.726	0.042	2.4	0.913	0.024	2.7	1.380	0.040	2.9	−9.5	8.7				
	127302_6	1.590	0.023	1.4	0.823	0.014	1.7	1.088	0.041	3.8	18.6	4.7				
	127302_11	1.467	0.023	1.6	0.756	0.028	3.7	1.231	0.014	1.1	44.3	4.9				
	127302_8	1.659	0.049	3.0	0.794	0.024	3.0	1.149	0.014	1.2	4.3	10.1				
	127303_10	1.672	0.027	1.6	0.844	0.016	1.9	1.098	0.017	1.5	1.6	5.6	1.6	1.672	1.098	34.5
	127329_2	1.513	0.012	0.8	0.606	0.017	2.8	1.145	0.015	1.3	34.8	2.5	33.0	1.521	1.146	34.5
	127329_5	1.481	0.023	1.6	0.708	0.011	1.5	1.17	0.012	1.0	41.2	4.8				
	127329_8	1.569	0.024	1.5	0.549	0.006	1.1	1.124	0.012	0.9	23.1	5.0				
Nevado																
	123957_1	1.527	0.045	2.9	0.567	0.013	2.3	1.308	0.042	3.2	31.8	9.3	31.8	1.527	1.308	35.5
	123955_1	1.415	0.020	1.4	0.919	0.010	1.1	1.185	0.004	0.4	55.0	4.2	47.9	1.450	1.203	35.5

Table 3 continued

Volc. field	Sample ID	100 Mn/Fe	2σ[1]	2σ (%)	Ni/(Mg/Fe)/1000	2σ	2σ (%)	100Ca/Fe	2σ	2σ (%)	Xpx (%)	2σ	Xpx avg (%)	100Mn/Fe avg	100Ca/Fe avg	S Latitude
	123955_3	1.481	0.023	1.6	0.800	0.014	1.7	1.277	0.023	1.8	41.2	4.8				
	123955_8	1.464	0.016	1.1	0.790	0.018	2.2	1.244	0.013	1.1	44.7	3.3				
	123955_9	1.438	0.038	2.7	0.941	0.028	3.0	1.105	0.024	2.2	50.2	7.9				
	126221_2a	1.470	0.019	1.3	0.792	0.009	1.1	1.082	0.017	1.6	43.6	3.9	39.8	1.488	1.152	36.0
	126221_3	1.548	0.023	1.5	0.614	0.014	2.3	1.161	0.017	1.5	27.4	4.8				
	126221_8	1.534	0.016	1.0	0.697	0.005	0.7	1.134	0.012	1.1	30.3	3.3				
	126221_2b	1.458	0.033	2.3	0.721	0.011	1.5	1.214	0.035	2.9	46.0	6.8				
	126221_10	1.431	0.024	1.7	0.722	0.01	1.4	1.168	0.038	3.3	51.6	5.0				
Llancanelo																
	123903_10	1.452	0.030	2.1	0.648	0.024	3.7	1.214	0.009	0.7	47.3	6.2	54.9	1.415	1.297	35.7
	123903_2	1.408	0.017	1.2	0.783	0.018	2.3	1.356	0.030	2.2	56.4	3.4				
	123903_3	1.428	0.021	1.5	0.642	0.028	4.4	1.341	0.014	1.1	52.3	4.4				
	123903_8	1.414	0.025	1.8	0.750	0.014	1.8	1.292	0.026	2.0	55.1	5.3				
	123903_9	1.375	0.023	1.7	0.851	0.012	1.4	1.283	0.033	2.6	63.3	4.9				
	123905_1	1.358	0.024	1.8	0.799	0.010	1.3	1.334	0.014	1.0	66.7	5.0	69.1	1.347	1.327	35.7
	123905_2	1.335	0.037	2.8	0.883	0.004	0.5	1.319	0.028	2.1	71.5	7.7				
Río Colorado																
	126175_8a	1.335	0.033	2.5	0.696	0.016	2.3	1.506	0.029	1.9	71.6	6.8	76.0	1.314	1.441	37.3
	126175_8b	1.359	0.026	1.9	0.696	0.014	2.0	1.563	0.027	1.7	66.5	5.4				
	126175_9a	1.290	0.011	0.9	0.775	0.053	6.8	1.485	0.064	4.3	80.7	2.3				
	126175_9b	1.308	0.024	1.8	0.794	0.006	0.8	1.434	0.015	1.0	77.0	5.0				
	126175_9c	1.349	0.042	3.1	0.815	0.023	2.8	1.504	0.045	3.0	68.5	8.7				
	126175_10a	1.288	0.033	2.6	0.849	0.015	1.8	1.295	0.010	0.8	81.2	6.8				
	126175_10b	1.265	0.020	1.6	0.852	0.017	2.0	1.297	0.021	1.6	86.0	4.1				
	Average 2σ		0.026			0.014			0.024			5.2				

Table 4 Major and trace element compositions of Payenia lavas

Field	Northern segment volcanic field									Nevado VF			Llancanelo VF		Río Colorado
Area	Huaiqueria		Papagayos			Rodeo									
Volcano	Huaiqueria	Huaiqueria	Guadaloso	Papagayos	Loma del Medio	Chico	E of Medio	E of Medio	Medio	Las Vegas	Amerillo	Fiero	Malacara	Malacara	Morado
Latitude	−34.06967	−34.07892	−34.31103	−34.30915	−34.49523	−34.46767	−34.47785	−34.47785	−34.48252	−35.46593	−35.51408	−35.98833	−35.70942	−35.72188	−37.30422
Longitude	−68.75432	−68.72707	−69.06522	−69.07373	−69.23267	−68.88417	−68.8423	−68.8423	−68.87258	−68.77778	−68.76137	−69.06427	−69.46313	−69.45377	−69.0184
Sample no.	127318	127322	127310	127309	127305	127304	127302	127303	127329	123957[a]	123955[a]	126221[a]	123903[a]	123905[a]	126175[a]
Major elements recalculated on a volatile-free basis															
SiO_2 (wt%)	45.91	45.86	45.25	45.85	47.83	46.87	45.57	45.92	47.15	46.45	47.32	46.06	46.98	46.78	46.49
TiO_2	1.47	1.46	1.19	1.23	1.28	1.60	1.33	1.32	1.33	1.37	1.44	1.46	1.54	1.53	1.63
Al_2O_3	15.46	15.43	13.81	14.18	15.55	14.95	14.94	15.04	14.60	15.14	15.04	14.65	15.08	15.02	13.72
$Fe_2O_3^{total}$	10.70	10.82	11.41	11.34	10.41	11.32	11.43	11.23	10.53	10.92	11.28	10.11	11.04	11.13	11.20
MnO	0.19	0.18	0.18	0.18	0.18	0.18	0.20	0.20	0.17	0.163	0.165	0.160	0.157	0.159	0.150
MgO	10.55	10.27	14.56	13.41	10.87	11.03	11.23	10.74	11.58	9.99	10.01	10.17	10.04	10.00	13.00
CaO	11.19	11.22	10.97	11.26	9.91	10.13	11.19	10.84	10.54	10.38	9.46	10.54	10.02	9.97	7.20
Na_2O	3.13	3.29	2.15	2.24	2.95	2.88	2.82	2.85	2.97	3.15	3.32	3.24	3.27	3.26	3.63
K_2O	1.43	1.48	0.97	0.86	1.43	1.31	1.18	1.15	1.34	1.02	1.27	1.42	1.00	0.99	1.78
P_2O_5	0.83	0.84	0.36	0.36	0.42	0.61	0.56	0.55	0.45	0.456	0.440	0.620	0.417	0.420	0.460
L.O.I.	0.5	0.1	1.9	1.8	1.9	0.4	0.9	0.5	1.0	0.26	0.00	1.10	0.09	0.05	0.20
Sum	99.46	99.78	99.42	99.74	99.78	99.50	99.53	99.44	99.50	99.30	99.58	99.58	99.62	99.30	99.58
Mg#[b]	68.45	67.63	73.74	72.24	69.7	68.20	68.37	67.79	70.76	66.80	66.14	68.89	66.68	66.42	71.87
FeO^{calc}	8.50	8.76	9.24	9.18	8.43	9.17	9.26	9.09	8.52	8.85	9.13	8.19	8.94	9.02	9.07
Sc (ppm)	30.9	31.53	29.46	30.66	29.74	30.18	27.10	26.92	24.10	28.00	24.68	26.14	26.01	22.19	17.19
V	263	268	255	278	245	257	241	241	227	231	223	242	221	198	148
Cr	375	362	774	777	436	453	510	489	562	407	378	434	484	238	484
Mn	1480	1496	1330	1395	1336	1429	1515	1545	1261	1377	1383	1170	1244	1200	1208
Co	46.33	45.20	56.25	55.80	45.85	49.10	46.17	45.89	46.28	51.59	50.78	43.69	49.72	55.98	60.04
Ni	184	175	333	300	199	225	234	227	256	202	240	205	212	135	428
Cu	56.23	57.26	66.92	61.03	38.36	57.01	58.76	53.90	52.60	58.86	56.22	54.90	59.31	47.46	53.24
Zn	75	79.67	70	75.76	70.15	83	80	81	72.46	72.78	76.31	70.88	81.92	92.87	84.92
Ga	19.1	19.92	16.3	18.13	18.45	18.9	19.2	19.7	18.83	19.21	20.01	19.31	19.09	19.99	17.89
Rb	33.7	35.86	15.4	13.11	36.52	27.3	30.6	29.6	33.04	21.63	27.61	35.32	18.55	19.15	38.82
Sr	1210	1180	777	1327	737	806	880	927	762	813	859	910	708	521	725
Y	28.92	29.30	16.29	17.52	21.19	25.36	22.64	22.89	18.15	23.91	23.31	22.98	21.82	22.42	20.13
Zr	171	175	85	97	130	156	137	138	128	128	138	142	138	120	184
Nb	20.40	20.97	6.93	7.61	11.82	14.67	10.62	10.84	12.69	13.97	14.19	19.00	15.21	9.39	34.21
Cs	2.34	2.59	0.71	0.87	2.33	1.55	1.73	1.56	1.38	0.83	1.01	1.32	0.69	0.60	1.09
Ba	777	816	411	505	510	562	587	568	527	512	562	607	381	424	500
La	40.34	43.04	19.33	22.17	24.46	27.95	35.73	36.87	26.31	24.25	25.29	30.09	19.98	17.13	24.94

Table 4 continued

Field	Northern segment volcanic field									Nevado VF			Llancanelo VF		Río Colorado
Area	Huaiqueria		Papagayos			Rodeo									
Volcano	Huaiqueria	Huaiqueria	Guadaloso	Papagayos	Loma del Medio	Chico	E of Medio	E of Medio	Medio	Las Vegas	Amerillo	Fiero	Malacara	Malacara	Morado
Ce	80.57	82.19	39.68	45.21	48.65	55.54	68.96	71.22	52.00	49.48	51.95	61.32	42.66	35.79	48.68
Pr	10.08	10.41	5.46	6.11	6.38	7.39	8.89	9.20	6.42	5.81	6.31	7.63	5.83	4.75	5.87
Nd	40.94	42.78	23.50	26.02	26.58	31.24	36.20	37.67	27.63	24.30	26.13	31.84	24.87	20.35	24.02
Sm	8.14	8.48	4.89	5.39	5.52	6.56	7.11	7.30	5.56	5.35	5.68	6.73	5.42	4.79	5.14
Eu	2.38	2.369	1.35	1.472	1.535	1.87	1.90	1.99	1.54	1.687	1.652	2.005	1.660	1.547	1.703
Gd	7.59	7.74	4.46	4.88	5.20	6.42	6.40	6.61	5.03	5.40	5.40	6.27	5.20	5.03	5.10
Tb	1.056	1.096	0.623	0.685	0.740	0.916	0.888	0.917	0.70	0.778	0.793	0.883	0.755	0.769	0.734
Dy	5.34	5.78	3.34	3.59	4.14	4.94	4.61	4.80	3.73	4.38	4.52	4.46	4.11	4.39	3.96
Ho	1.037	1.039	0.589	0.634	0.753	0.919	0.802	0.821	0.64	0.814	0.794	0.821	0.777	0.820	0.719
Er	2.72	2.88	1.59	1.65	2.04	2.46	2.08	2.14	1.75	2.19	2.21	2.18	2.07	2.21	1.88
Tm	0.425	0.409	0.222	0.225	0.288	0.361	0.278	0.279	0.24	0.327	0.313	0.284	0.291	0.315	0.242
Yb	2.52	2.43	1.25	1.33	1.76	2.04	1.67	1.67	1.49	1.96	1.82	1.79	1.77	1.91	1.54
Lu	0.383	0.380	0.186	0.199	0.262	0.311	0.242	0.252	0.21	0.290	0.259	0.271	0.269	0.283	0.220
Hf	4.11	4.06	2.36	2.50	3.17	3.74	3.36	3.44	3.20	2.96	3.28	3.32	3.24	2.98	3.87
Ta	1.088	1.135	0.391	0.413	0.684	0.823	0.608	0.609	0.74	0.672	0.745	1.006	0.829	0.612	1.957
Pb	11.39	10.80	4.13	6.89	3.57	7.46	8.88	8.90	8.28	6.16	7.05	8.44	4.45	5.23	3.29
Th	8.20	9.08	4.46	5.19	5.64	5.27	8.45	8.94	6.67	4.47	4.87	5.06	2.94	3.41	3.51
U	2.23	2.33	0.84	1.03	1.49	1.47	1.58	1.66	1.77	1.20	1.12	1.27	0.81	0.87	1.00

[a] From Søager et al. (2013)

[b] Mg# is calculated assuming $Fe^{2+}/Fe_{total} = 0.9$

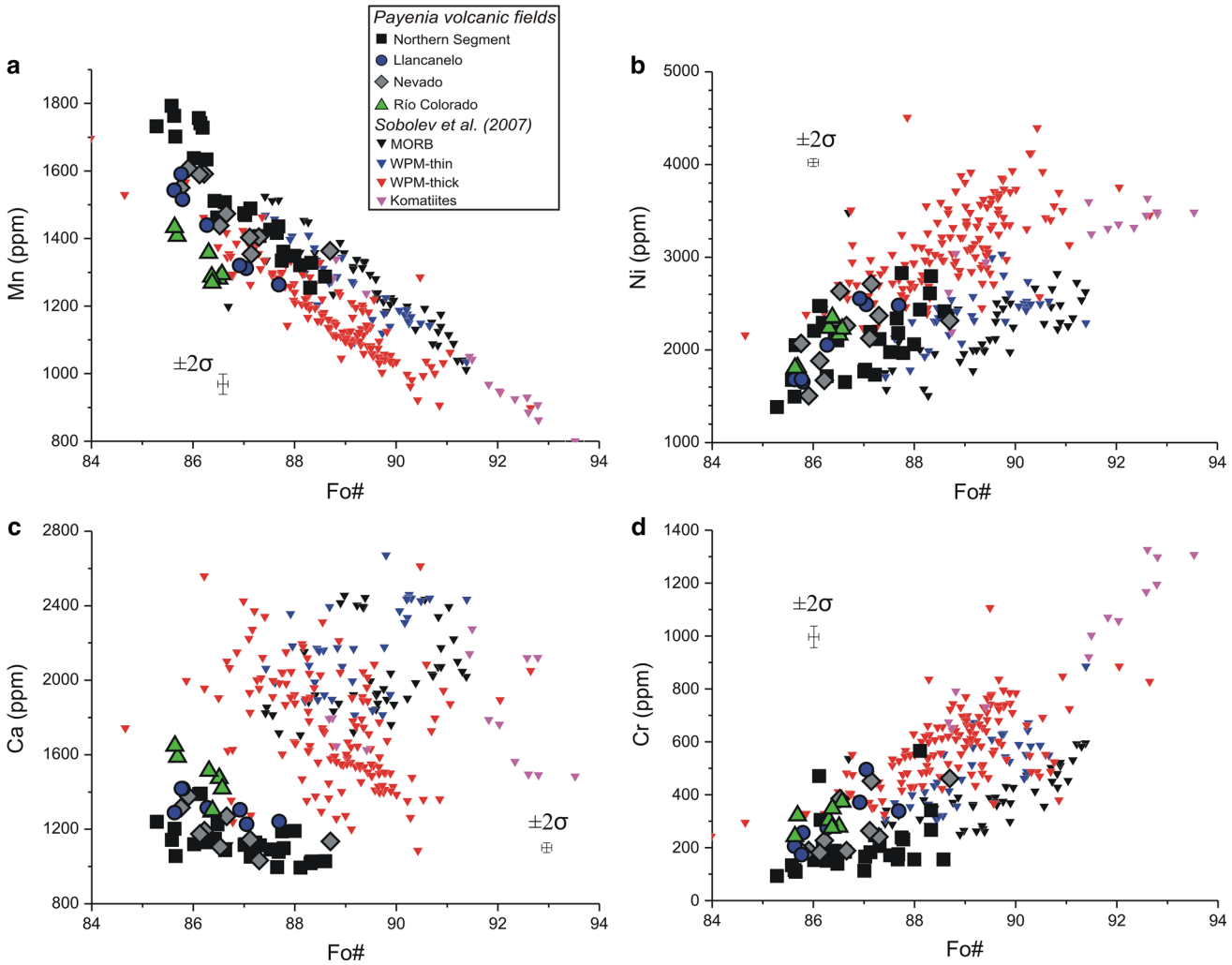

Fig. 2 High-precision minor element concentrations of Mn, Ni, Ca and Cr in primitive olivine phenocryst cores in Payenia basaltic rocks versus Fo#: **a** Mn, **b** Ni, **c** Ca, **d** Cr. Data from Sobolev et al. (2007) are shown for comparison and divided into WPM (within plate margins)—thick, WPM-thin, MORB and Komatiites

is characterized by relatively high Ba/Th and Eu/Eu* ratios (142 and 1.02, respectively) and, e.g., low Th/Nb, La/Nb and Th/La ratios (0.1, 0.73 and 0.14, respectively). The northern samples have relatively low Ba/Th and Eu/Eu* ratios (as low as 63.7 and 0.86, respectively) and relatively high Th/Nb, La/Nb and Th/La ratios (up to 0.8, 3.5 and 0.25, respectively) characteristic of the northern SVZ arc volcanism (Holm et al. 2014).

Discussion

Crystal–melt relations

The high Mg# and MgO of the rocks together with their magnesian olivine phenocrysts indicate that only olivine and chromite crystallized in these basaltic magmas, as is also the main indication from petrography. Assuming that these minerals were the only fractionating phases, the MgO variation among the investigated samples can be explained by a limited fractionation of <7% olivine from parental mantle melts with ~Mg# = 72–74 (Fig. 3a; Table 4). In Fig. 3a, variation of calculated olivine compositions as the result of olivine fractionation of magma with a composition as sample 127304 is modelled by incremental subtractions of equilibrium olivine. Equilibrium olivines were calculated using the Herzberg and O'Hara (2002) model and using a $Kd_{Mg}^{ol/melt}$ equation from Beattie et al. (1991). The $100Mn/Fe_{ol}$ ratio is minimally influenced by olivine fractionation as previously established by Sobolev et al. (2007) and Herzberg (2011). Similarly, fractionation of clinopyroxene has been modelled showing that Mn/Fe in co-precipitating olivine will decrease significantly during clinopyroxene fractionation. More than 15% clinopyroxene fractionation would be required to

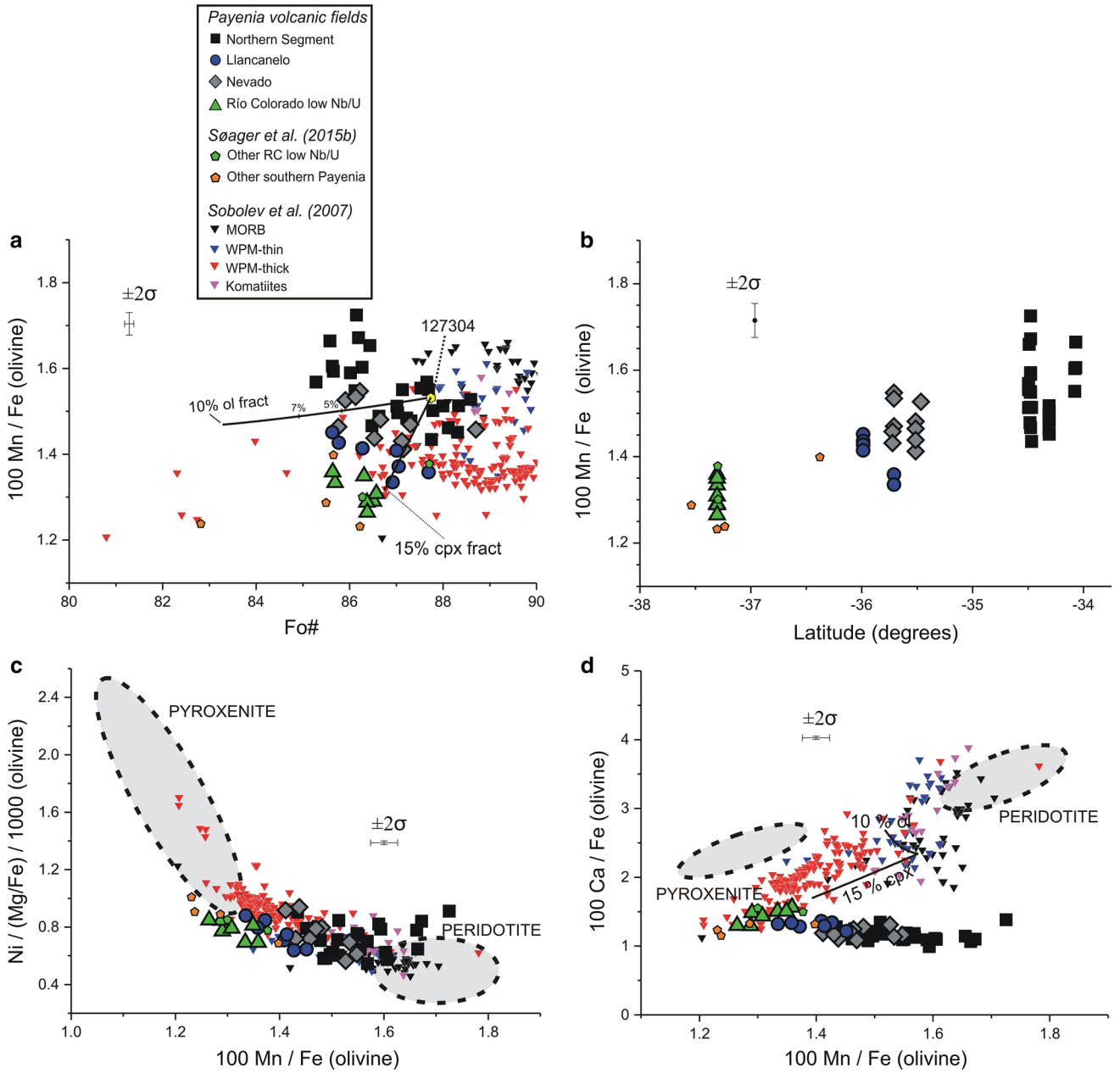

Fig. 3 **a** Olivine Mn/Fe versus Fo#. The change of composition of olivines crystallizing from melts experiencing olivine and clinopyroxene fractionation is indicated by the *modelled curves* (see text under "Discussion" section). **b** $Mn/Fe_{olivine}$ versus geographical latitude. The Mn/Fe ratio in olivine increases northward in Payenia magmas. See text under "Discussion" section. **c** Olivine Ni/(Mg/Fe) versus Mn/Fe. **d** Olivine Ca/Fe versus Mn/Fe. The new high-precision phenocryst data are displayed together with average olivine compositions with Fo# >82 of southern Payenia of Pleistocene uncontaminated samples from Søager et al. (2015b). Data from Sobolev et al. (2007) are shown for comparison. *Gray ellipses* outline equilibrium olivine compositions from experimentally derived pyroxenite and peridotite melt compositions of Sobolev et al. (2007). Average ± 2σ uncertainties for the new data are shown in (**a**)–(**d**) and for individual phenocrysts in Table 3

explain the observed variation in Mn/Fe_{ol} along the backarc. Although clinopyroxene phenocrysts are present in some rocks, this phase did not fractionate significantly, as demonstrated by the lack of decrease of 100Ca/Fe with decreasing $100Mn/Fe_{ol}$ (Fig. 3d). We also note that the few samples with clinopyroxene (and minor amount of plagioclase) are from the Northern Segment and are among the most calcic, which indicates that these phases had not fractionated significantly. Magnetite fractionation would affect the Mn/Fe ratio, but high TiO_2 and V contents in all samples contradict such fractionation, as well as the fact that no phenocrysts were observed.

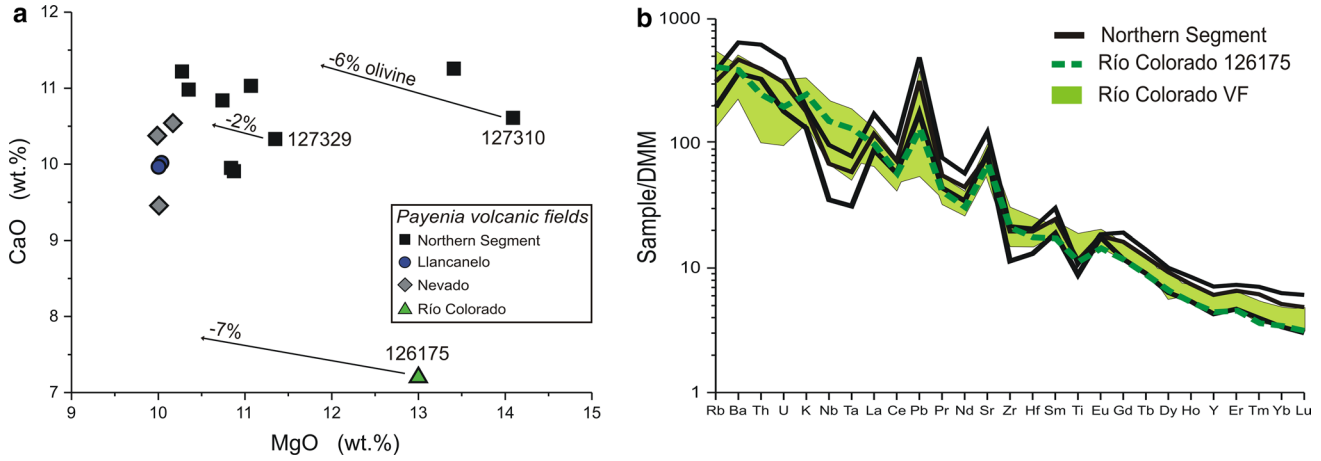

Fig. 4 **a** CaO versus MgO for the host basalts. Three samples (126175, 127329 and 127310) have been corrected for 7, 2 and 6% olivine accumulation, respectively, by subtracting the most primitive olivine compositions analyzed with high precision from the whole-rock composition until olivine–melt equilibrium. **b** Depleted MORB mantle (Salters and Stracke 2004) normalized spider diagrams for Northern Segment samples showing arc characteristic trace element signatures. Río Colorado sample 126175 is presented together with the Río Colorado compositional field from data of Søager et al. (2013) (*green field*), all with an OIB-type enrichment pattern. Llancanelo samples have intermediate enrichment patterns

Olivine compositions measured in sample 126175 from Río Colorado and 127329 and 127310 from the Northern Segment are significantly less magnesian than the expected $Fo_{90\text{-}89}$ for melts with Mg# = 74–71 of the whole rocks (wr) according to the olivine–liquid exchange coefficient $K_D = (Fe/Mg)^{ol}/(Fe/Mg)^{melt} = 0.30 \pm 0.03$ of Roeder and Emslie (1970) (Fig. 5). An explanation of this by magma mixing would require a component exceptionally magnesian for the province, and therefore olivine accumulation is the likely cause. Subtraction of the most primitive olivine composition in each sample in amounts of 7, 6 and 2% for samples 126175, 127310 and 127329, respectively, changed the wr compositions to be within error of equilibrium with the olivines (Supplementary material 5), and these corrected wr compositions will be used onward (Figs. 4, 5).

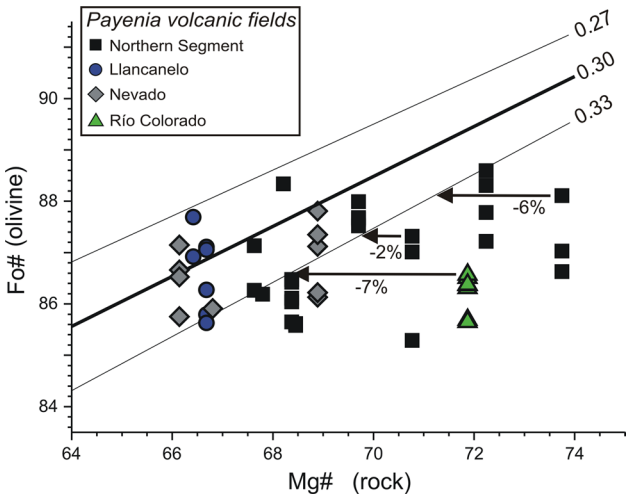

Fig. 5 $Fo^{\#}$ (olivine) versus Mg# (rock) for olivine phenocryst cores. *Solid lines* represent the $Kd^{olivine\text{-}liquid}_{Fe/Mg}$ equilibrium of 0.3 ± 0.03 of Roeder and Emslie (1970). $Mg^{\#}$ calculated with $Fe^{2+}/Fe^{tot}_{rock} = 0.9$. For most analyzed samples, olivine is indicated to have been in equilibrium with the host rock magma. The effects of correction for olivine accumulation in three samples (126175, 127329 and 127310) are shown. See text under "Discussion" section

Source chemistry

Because of the primitive composition of all rocks considered here, processes such as assimilation and fractional crystallization are expected to have had little importance for the magmas. In particular, the rocks selected for this study were previously screened for effects of crustal contamination (Søager et al. 2013, 2015a; Søager and Holm 2013; Holm et al. 2016), which is thus considered insignificant.

The southward decrease in Mn/Fe_{ol} is accompanied by an increase in host rock Nb/U from 5–10 to 20–54 (Fig. 6) which describes the arc-type to OIB-type incompatible trace element variation in Payenia (Søager et al. 2013, 2015b; Søager and Holm 2013). The correlation between trace element compositions and source lithology can be recognized in correlations between the sample average Mn/Fe_{ol} and many whole-rock trace element ratios (Fig. 7; see also Søager et al. 2015b). Since ratios of very incompatible elements in the common mantle minerals (e.g., La, Nb, Ba and Th) do not change during melting or early fractional crystallization, the variations in Fig. 7 reflect geochemical differences in the mantle source regions. The arc-type

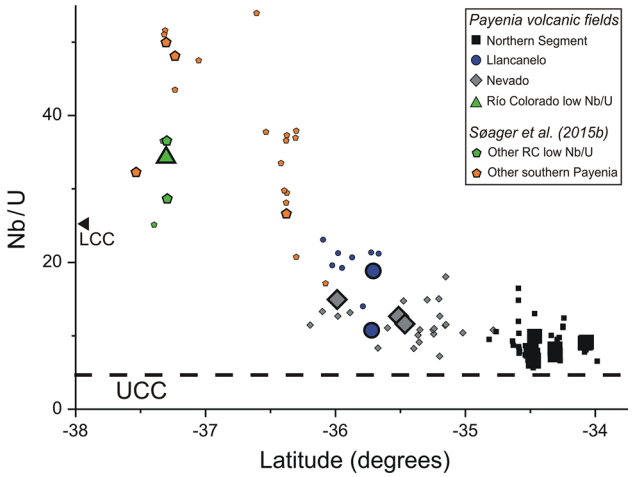

Fig. 6 **a** Rock Nb/U versus degree latitude (°S). Payenia samples additional to those already presented above from Søager et al. (2013, 2015a, b) and Holm et al. (2016) are plotted with the *smallest symbols* for comparison. Río Colorado samples with low Nb/U according to Søager and Holm (2013) have been identified

trace element enrichment in magmas of the Northern Segment indicates that these dominantly peridotite melts were derived from a metasomatized upper mantle, as discussed by Søager et al. (2013, 2015b) and Holm et al. (2016). Although fluid enrichment may be important, this cannot on its own explain the trace element variation observed, and specifically the relatively low Eu/Eu*, Ba/Th and high Th/La ratios found in the northernmost samples in the backarc and arc support the presence of an UCC component in the mantle source (e.g., Holm et al. 2014, 2016; Søager et al. 2015a). Rocks of magmas that have experienced feldspar fractionation, such as granites (main constituent of UCC), have low Eu/Eu* ratios, and the lowest Eu/Eu* ratio measured is 0.86 in sample 127302 from the Rodeo Group in the Northern Segment. This ratio gradually increases with decreasing Mn/Fe_{ol} to values up to 1.08 in the Río Colorado samples (Fig. 7a). The positive Eu anomaly is likely the result of small amounts of LCC in the Río Colorado source (Kay et al. 2013; Søager and Holm 2013) as is also proposed for other EM1 magmas (e.g., Willbold and Stracke 2006). Moreover, the Th/La ratio increases from a value of 0.08 at Río Colorado northward to 0.25 in sample 127329 from the Rodeo Group (Figs. 7b, 8). This increase is not characteristic of fluid enrichment since La is more mobile in fluids than Th (Kogiso et al. 1997; Kessel et al. 2005), and therefore it is more likely a feature that can be ascribed to the enrichment of the mantle by melts of UCC or sediments (Plank 2005). We also note, like Søager et al. (2015b), that Ba/Th ratios correlate negatively with Mn/Fe_{ol} and decrease northward (Fig. 7c). This strongly supports the suggestion that the Northern Segment mantle source was enriched by UCC during subduction because (1) Ba is much more mobile in fluids than Th (Kogiso et al. 1997; Kessel et al. 2005) and (2) Ba is compatible in amphibole, biotite and k-feldspar and is removed from the magmas during fractionation of evolved magmas, whereas Th is incompatible. Th is therefore relatively enriched compared to Ba in many granitic rocks. Ba/Th ratios in magmas of the Northern Segment are as low as mean UCC values (Rudnick and Gao 2003), whereas trench sediments from Lucassen et al. (2010) and Jacques et al. (2013) extend to much higher Ba/Th ratios. Northward increasing upper crustal signatures in the SVZ arc rocks have been argued to arise from increasingly high rates of forearc subduction erosion and pointed out to be in contrast to a northward decrease (from 40°S to 36°S) in the thickness of sediments in the Chile trench (Holm et al. 2014; Kay et al. 2005; Stern 1991, 2011). Overall, incompatible trace element ratios in Northern Segment magmas approach mean UCC of Rudnick and Gao (2003) with La/Nb = 2.6, Th/La = 0.33, Th/Nb = 0.87 and low Ba/Th = 59, Nb/U = 4.4 and Eu/Eu* = 0.7 (Fig. 7). The correlation between trace element ratios and Mn/Fe_{ol} can simply be explained by two-component mixing trends from north to south as also suggested by Søager et al. (2015b).

Possible causes for variation of Mn/Fe_{ol}

Because the Mn/Fe_{ol} ratio changes less than the $Ni/(Mg/Fe)_{ol}$ parameter during olivine fractionation below Fo_{90} (Sobolev et al. 2007), we prefer to use the Mn/Fe_{ol} ratio as indicator for the amount of pyroxenite melt in the magmas. The observed northward increase of Mn/Fe^{2+}_{ol} (Fig. 3b) is accompanied by a steady and similar increase of Mn and a decrease of Ca/Fe_{ol} (Fig. 3d). Therefore, the rise of Mn/Fe_{ol} is not primarily caused by an increase in the oxidation state of iron in the magmas, because that would cause Ca/Fe to increase as well due to the lower amounts of Fe^{2+} in the magmas. We also note that the effect of oxidation on manganese would not result in a northward increase in Mn/Fe^{2+}_{ol}, as is observed in Payenia, due to lower amounts of Mn^{2+} in the magmas.

Adding subduction zone fluids and upper continental crust (UCC) to the mantle source will have little effect on the Mn/Fe^{tot} ratio in the melt produced, because UCC and melts thereof have low contents of Fe and Mn and have Mn/Fe^{tot} ratios ($100Mn/Fe^{tot}$ = 1.5–2.0) in a number of UCC compositions listed by Rudnick and Gao (2003) within the peridotite–pyroxenite range (100Mn/Fe = 1.1–2.1) of experimental melts presented in Sobolev et al. (2007).

Experimental evidence suggests only minimal fractionation of Mn/Fe_{melt} during peridotite partial melting (Humayun et al. 2004; Walter, 1998; Le Roux et al. 2011) if the melting degree does not approach 0% (Davis et al. 2011). Contrary to this, increasing partial melting of pyroxenite will increase

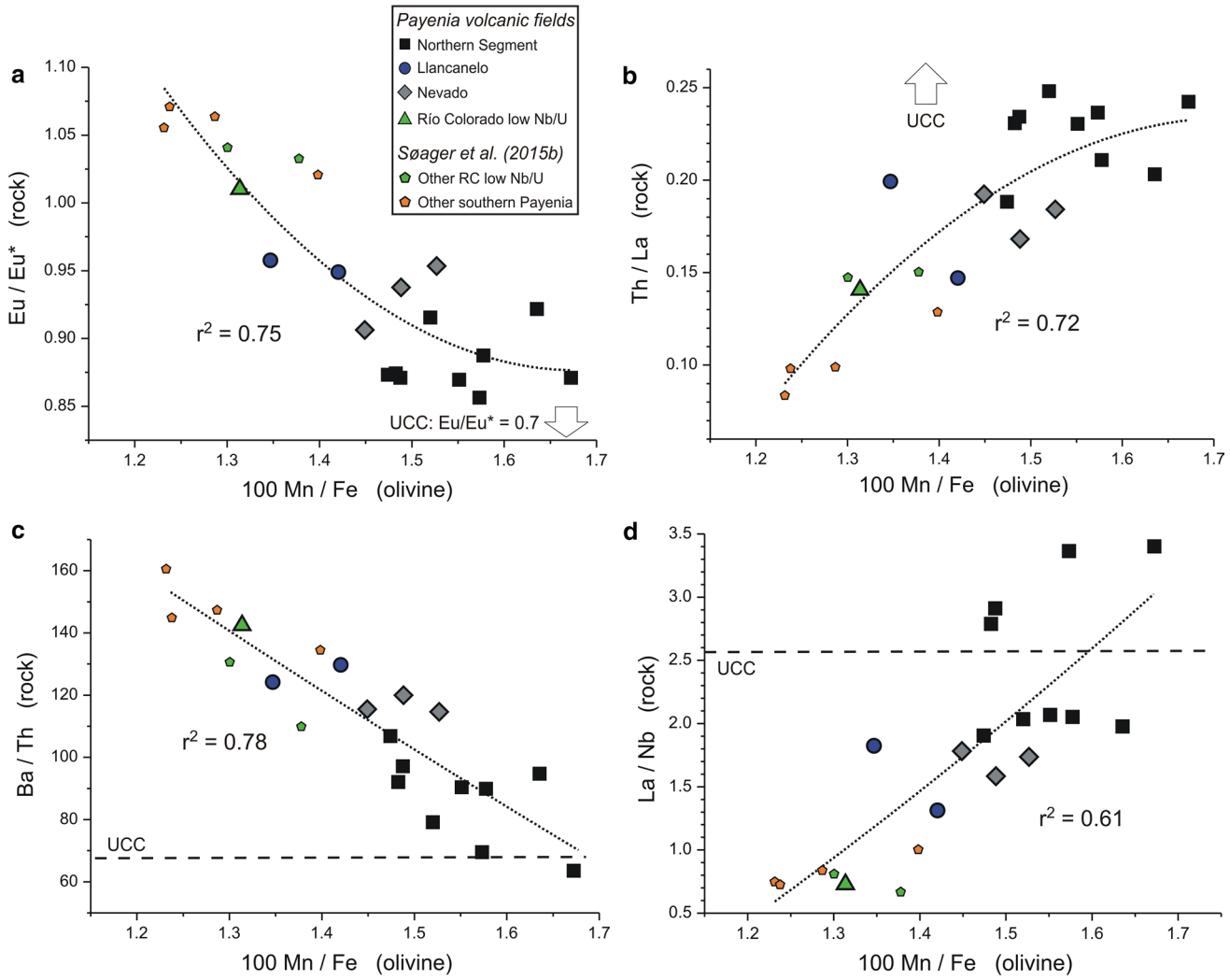

Fig. 7 Selected rock trace element ratios and Eu/Eu* versus Mn/Fe of sample average olivine core compositions. $Eu/Eu^* = Eu_N/\sqrt{Sm_N * Gd_N}$. Normalization according to the CI chondrite composition of McDonough and Sun (1995). The composition of average upper continental crust, UCC (Rudnick and Gao, 2003), is indicated by *arrows* or a *stippled line*. Sample average Mn/Fe_{ol}: Table 3. Correlation curves (*dotted*) and coefficients (r^2) are discussed in the text

the Mn/Fe ratio in the melt (e.g., Sobolev et al. 2007; Herzberg 2011), and pyroxenite-derived melts are therefore most easily distinguished from peridotite-derived melts at lower degrees of partial melting (Sobolev et al. 2007; Herzberg 2011). The low Mn/Fe ratios in southern Payenia, thus, tend to conservatively reflect the pyroxenite component in the source. Dy/Yb_{PM} ratios in the studied rocks range from 1.4 to 1.9 and show no correlation with Mn/Fe_{ol} (not shown) indicating that variation in mantle lithology was more important than pressure-related mineralogical changes for the Mn/Fe variation in mantle melts along Payenia.

Summing up, we therefore attribute the variation of Mn/Fe^{2+}_{ol} to mixing of melts derived from mantle sources with different lithologies as suggested by Sobolev et al. (2007).

Olivine–melt partitioning of Mn/Fe

The partition coefficient for Fe and Mn between olivine and a coexisting melt depends on the melt composition, temperature, pressure and oxygen fugacity at olivine crystallization (e.g., Evans et al. 2012; Ford et al. 1983; Herzberg and O'Hara 2002; Mysen 2007). Le Roux et al. (2011) showed that melt temperature differences of 1300–1500 °C and 1.5–2 kbar pressure crystallization will affect $Kd^{ol/melt}_{Mn}$ and $Kd^{ol/melt}_{Fe}$ equally. Thus, we do not expect any significant along backarc fractionation in $Kd^{ol/melt}_{Mn/Fe}$ due to variable temperatures or pressures during olivine crystallization. The effect of variable melt composition on the partition coefficients for Fe and Mn between olivine and melt has been calculated for the present

Payenia samples using the equations of Herzberg and O'Hara (2002) where $Kd_{Mg}^{ol/melt}$ were calculated according to Beattie et al. (1991). $Kd_{Mn/Fe}^{Ol/melt}$ was calculated for the most primitive whole rocks (wr) (sample 127309 with Mg# = 72, Table 4) and a less primitive wr (sample 126230 with Mg# = 64 from Søager et al. 2015b), which are shown as the upper limit and lower limit of the yellow field in Fig. 9a, respectively, and these encompass all studied samples. The two values show that the compositional difference in melt composition results in a ~0.05 difference in $100Mn/Fe_{ol}$. Thus, the observed differences in melt compositions can only explain a small fraction of the north-to-south Mn/Fe_{ol} variation in Payenia. Neither the decrease in Mn/Fe_{ol} expected from the less than 10% olivine fractionation can account for the large variation in Mn/Fe_{ol} along Payenia.

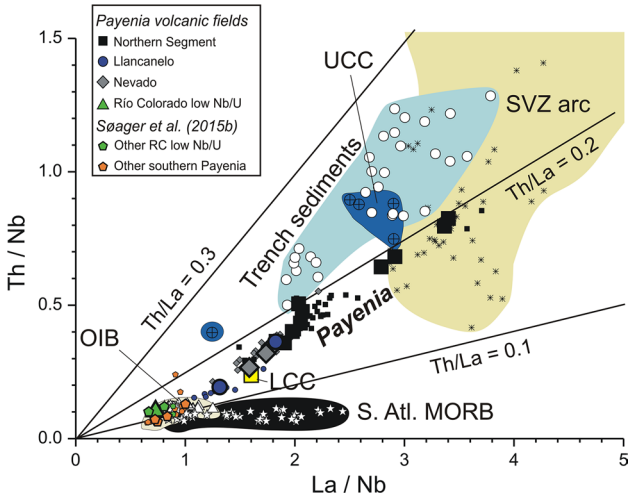

Fig. 8 Rock Th/Nb versus La/Nb. *Symbols* of Payenia rocks as in Fig. 6. Trench sediment data are from Lucassen et al. (2010) and Jacques et al. (2013). South Atlantic MORB with $(La/Sm)_N$ <1 (normalized to primitive mantle values of McDonough and Sun (1995)). South Atlantic MORB data are from Le Roux et al. (2002). Upper continental crust (UCC) values and average lower continental crust (LCC) are from Rudnick and Gao (2003) and references therein. Data from the Southern Volcanic Zone (SVZ) are from Holm et al. (2014) and Jacques et al. (2013)

Low-Ca subduction zone olivines

The strikingly low Ca and 100Ca/Fe in Northern Segment and Nevado olivines relative to the OIB-MORB array (Figs. 2c, 3d) are characteristic of olivines from subduction zone environments (e.g., Kamenetsky et al. 2006; Portnyagin et al. 2007; Wehrmann et al. 2014; Gavrilenko et al. 2016). However, in contrast to the pyroxenite-derived low-CaO melts of southern Payenia, the wr CaO contents of the host rocks are as high as expected for peridotite melts (~10–11 wt% in Northern Segment and Nevado rocks). Therefore, the northern and southern Payenia samples form a negatively correlated line in a plot of Ca/Fe_{wr}^{2+} versus Ca/Fe_{ol} (Fig. 9b) in contrast to the positively correlated trend expected from varying clinopyroxene/olivine ratios in the mantle source according to Sobolev et al. (2007). Olivines and wr from Payenia extend from an arc-type component

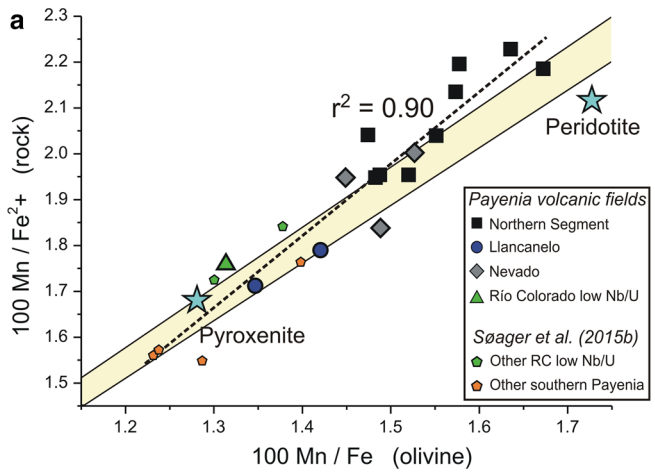

Fig. 9 **a** Mn/Fe^{2+} (rock) versus Mn/Fe (olivine), **b** Ca/Fe^{2+} (rock) versus Ca/Fe (olivine). *Symbols* as in Fig. 7. Samples 126175, 127310 and 127329 have been corrected for 7, 6 and 2% olivine accumulation, respectively. *Lines of yellow field* in (**a**) represent the calculated $Kd_{Mn/Fe}^{Ol/melt}$ equilibrium based on the melt composition of samples 127309 and 126230, which represent the total range of sample compositions. *Stars* are olivine in equilibrium with average experimental melts of Sobolev et al. (2007) (assuming $Fe^{2+}/Fe^{tot} = 0.9$) derived from pyroxenite and peridotite, respectively. See text under Discussion. In **b** the *yellow field* delimits the samples similarly as in (**a**). Field of SVZ is based on olivines with $Fo^{\#}$ >87 from Wehrmann et al. (2014). N-MORB melt composition is from Workman and Hart (2005), and the equilibrium olivine composition is calculated. Anhydrous peridotite melt and hydrous arc mantle melt are hypothetical

with low Ca/Fe_{ol} and high Ca/Fe^{2+}_{wr} to a pyroxenite-derived component with low Ca/Fe_{ol} with low Ca/Fe^{2+}_{wr} (Fig. 9b).

The melt compositional influence on the olivine–melt partitioning for Fe and Ca due to the variable melt compositions in Payenia has been calculated according to the model of Herzberg and O'Hara (2002) using the same two rock compositions as above for Mn/Fe and are shown as the limits of the yellow field in Fig. 9b. It is evident that the variation of primitive melt compositions in Payenia influences the Ca/Fe_{ol} insignificantly compared to the variation expected from melts of peridotite contra pyroxenite (Fig. 9b).

The low Ca contents of the northern backarc olivines must, thus, have been caused by lower partition coefficients for Ca in olivine, $D^{ol/melt}_{Ca}$. We have calculated $D^{ol/melt}_{Ca}$ for the samples in this study and the Pleistocene samples of Søager et al. (2015b) using wr compositions olivine accumulation/fractionation corrected to equilibrium with the average of the olivines with the highest Fo content. For the samples from this study, the values listed in Supplementary material 5 were used. For the samples from Søager et al. (2015b), the wr compositions were corrected for olivine fractionation using equilibrium olivine compositions in steps of 0.1% and a $Kd^{ol/melt}_{Fe/Mg} = 0.3$. For comparison, $D^{ol/melt}_{Ca}$ values for the most primitive olivines from the SVZ with Fo > 87 (Wehrmann et al. 2014) were calculated using the associated melt inclusion compositions given in Wehrmann et al. (2014). The results are all lower than the $D^{ol/melt}_{Ca} = 0.023–0.029$ calculated for the samples using the partition coefficient model from Herzberg and O'Hara (2002) (Fig. 10a), and the samples show a regular

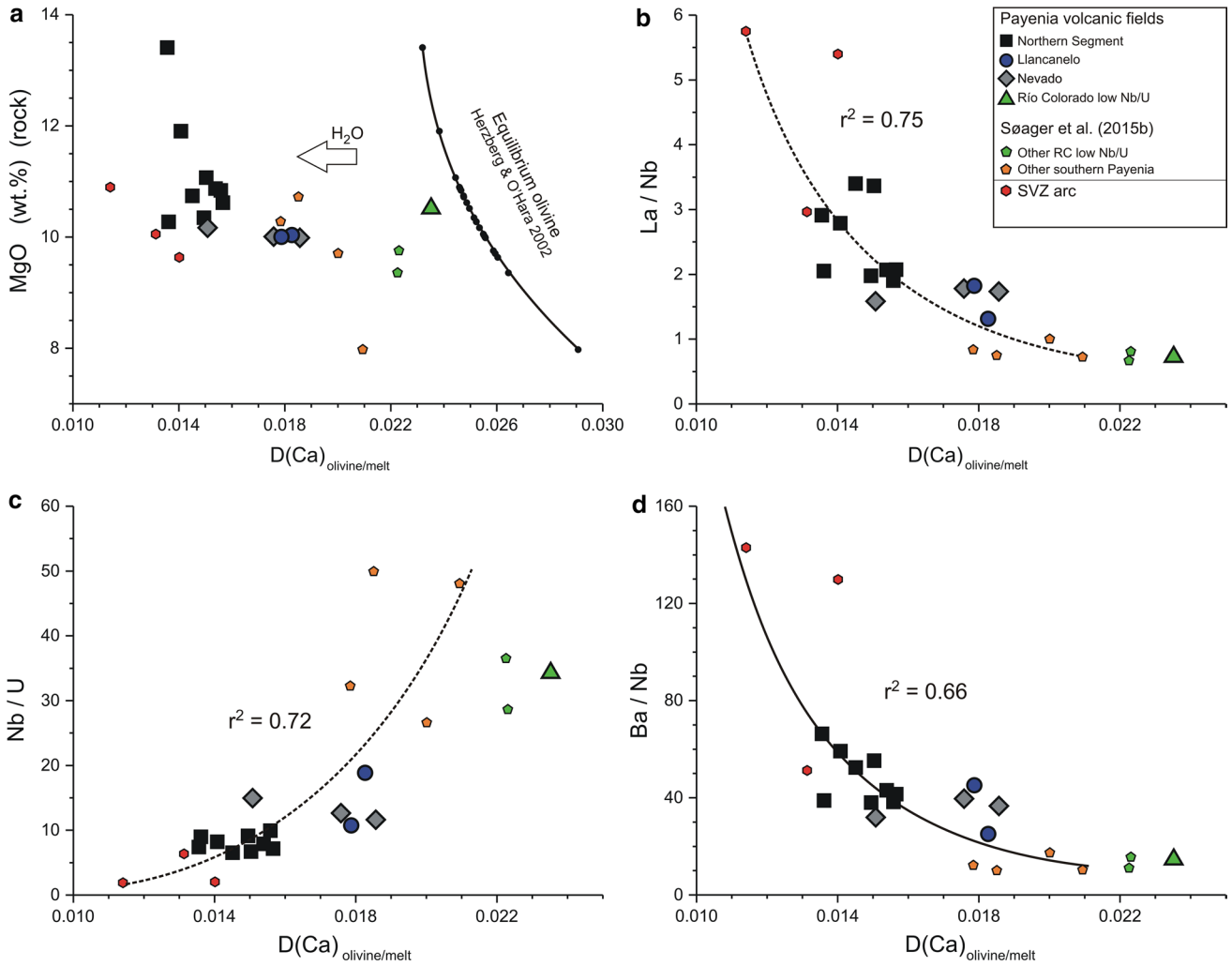

Fig. 10 **a** MgO, **b** La/Nb, **c** Nb/U, and **d** Ba/Nb versus $D^{ol/melt}_{Ca}$. In **a** the *black dots* in the *curve* show the anhydrous olivine partition coefficients for Ca calculated for each sample using the formulas from Herzberg and O'Hara (2002). Most samples fall in a narrow range in MgO, and the range in $D^{ol/melt}_{Ca}$ is proposed to be caused by varying H_2O contents as shown by the *arrow*. *Symbols* as in Fig. 7. SVZ arc data are from Wehrmann et al. (2014) with data points calculated as sample averages of the available olivine–melt inclusion pairs. Regression curves (*stippled*) and correlation coefficients (r^2) are shown in (**b**)–(**d**). See text under "Discussion" section

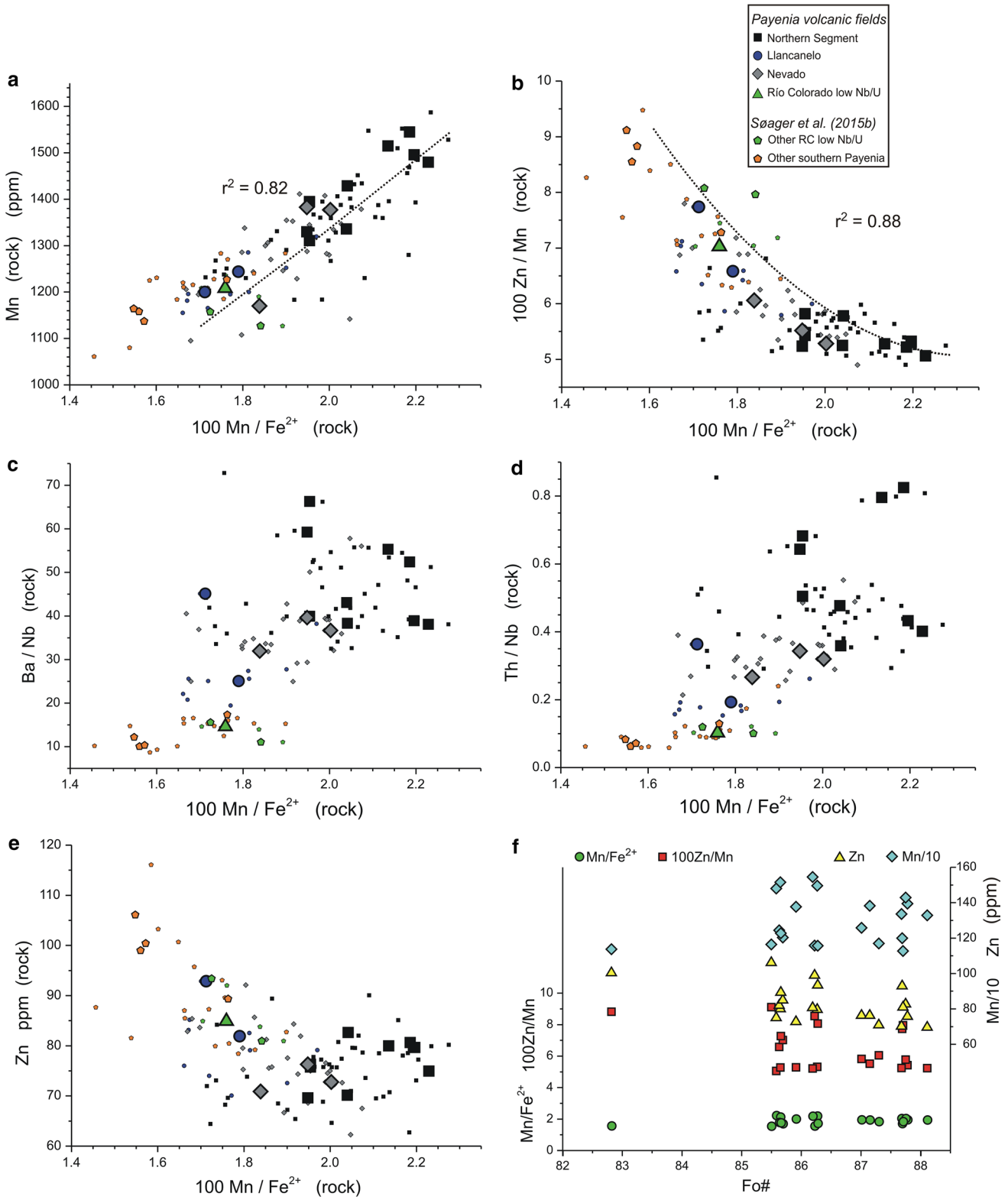

Fig. 11 **a** Mn, **b** Zn/Mn, **c** Ba/Nb, and **d** Th/Nb and **e** Zn versus Mn/Fe^{2+} for the host magmas. *Symbols* as in Fig. 6. In the primitive magmas, the minor elements Zn and Mn and their ratio display the same correlation with Mn/Fe^{2+} and north-to-south variation as documented by the primitive olivines. The north-to-south variation of incompatible elements in Payenia magmas is also correlated with rock Mn/Fe^{2+}. **f** Rock Mn/Fe^{2+}, Zn/Mn, Zn, and Mn versus sample average $Fo^{\#}$ indicate no correlation with olivine evolution

decrease in $D_{Ca}^{ol/melt}$ with increasing slab component, here represented by increasing La/Nb and Ba/Nb and decreasing Nb/U (Fig. 10b–d).

$D_{Ca}^{ol/melt}$ has been shown to be dependent on melt composition and temperature with olivines crystallizing in lower MgO and lower-temperature melts having higher $D_{Ca}^{ol/melt}$ (e.g., Libourel 1999; Feig et al. 2006; Mysen 2007). Also the alkali content of the melts was found to have a significant influence with higher alkali contents leading to higher $D_{Ca}^{ol/melt}$ (Libourel 1999). In contrast, $D_{Ca}^{ol/melt}$ has been shown to be largely independent on pressure and oxygen fugacity (e.g., Jurewicz and Watson 1988; Feig et al. 2006; Laubier et al. 2014). Since the majority of the investigated basalts fall within a narrow range in MgO (9–11 wt%) and $Na_2O + K_2O$ (4–5 wt%), different melt compositions cannot explain the main variation in $D_{Ca}^{ol/melt}$. However, the higher $D_{Ca}^{ol/melt}$ found for the low-Nb/U basalts relative to the other southern Payenia samples could be an effect of their higher alkali contents (5.6–6.6 wt% $Na_2O + K_2O$). Feig et al. (2006) suggested that $D_{Ca}^{ol/melt}$ is lowered by increasing H_2O contents in the melt and this would be a viable explanation for the lowered partition coefficients in the samples with highest slab component. We therefore suggest that the gradually decreasing $D_{Ca}^{ol/melt}$ is caused by an increasing fraction in the magmas of H_2O-rich peridotite melt formed by slab fluxing and that this explains the lower Ca/Fe in the olivines of these magmas relative to the MORB-OIB olivine trend in Fig. 3d. The lower $D_{Ca}^{ol/melt}$ indicated by the southern Payenia basalts relative to the anhydrous values calculated with the formula of Herzberg and O'Hara (2002) could suggest that the pyroxenite source also contains significant amounts of H_2O.

Pyroxenite and peridotite fraction from whole-rock compositions

The good positive correlation between average Mn/Fe in olivines and whole rocks (wr) ($r^2 = 0.90$ Fig. 9a) indicates approximate equilibrium. Also wr Mn and Zn/Mn correlate with Mn/Fe_{ol} (Fig. 11a, b). The Mn/Fe_{wr}^{2+} ratio is not affected much by olivine accumulation using FeO^{corr} (Supplementary material 5). The variation indicated in Figs. 9a and 11b cannot be explained by olivine fractionation since there is no correlation between $Fo^{\#}$ and whole-rock transition metal ratios (Fig. 11f). This supports earlier observations (Le Roux et al. 2010, 2011; Davis et al. 2013; Søager et al. 2015b) that elements compatible in olivine and pyroxenes can be used to identify the source from which a melt is derived, using primitive magma compositions. A correlation as displayed in Fig. 9a can be generated either if the oxidation states of all magmas are approximately the same or if the magmas are mixtures of two end-member compositions with different oxidation states. The variation in Mn/Fe_{wr}^{2+} is not related to a variation in the oxidation states of the melts, because all wr $100Mn/Fe^{2+}$ values are calculated with a constant ratio of $Fe^{2+}/Fe^{tot} = 0.9$ (Fig. 9). The variation in Mn/Fe_{wr} from south to north along the backarc is related to a northward increase in Mn and a northward decrease in FeO^T.

Minor elements in magnesian olivines are good indicators of mantle source lithology because they reflect the most primitive melt compositions. However, in our case, within single samples, large differences exist between the Mn/Fe_{ol} for different olivine phenocrysts (Table 3). Since no correlation is found between $Fo^{\#}$ and $(Mn/Fe)_{olivine}$ (Fig. 3a), the variation in Mn/Fe_{ol} indicates that olivine crystallized from different mantle melt batches that subsequently mixed en route to the surface. Thus, in the case of mixing of magmas derived from different source lithologies, the melt composition would give a more accurate estimate of the proportion of pyroxenite- to peridotite-derived melt components in a given rock sample than the individual olivine phenocrysts. The reason for the good positive correlation in Fig. 9a must be that for the investigated rocks, the average of several primitive olivine core compositions is fairly representative of the proportion of pyroxenite and peridotite in the mixed melt.

Conclusion

A clear north-to-south decrease in Mn/Fe in both primitive whole-rock (wr) and olivine compositions in the Payenia backarc basalts is caused by a decrease in Mn and an increase in Fe contents and cannot be explained by melt evolution, melting depths or oxidation states of the magmas. Instead, it suggests an increase in the fraction of pyroxenite-derived melts. This is coupled to a transition in trace element signatures from arc-like in rocks of the Northern Segment to OIB-like in rocks at Río Colorado. Good correlations between a range of wr incompatible trace element ratios, major and trace element concentrations and transition element ratios with Mn/Fe_{ol} and Mn/Fe_{wr} indicate that the variation is caused by mixing of melts from two distinct mantle sources. We consider the low Eu/Eu*, Ba/La and Ba/Th (0.86, 16 and 63) and high Th/La (0.25) in rocks of the Northern Segment as an indication that the source was enriched by upper continental crustal melts (UCC). Source mixing must involve two components, of which the northern is a peridotitic mantle enriched by fluids and UCC melts from the subducting slab and the southern is a pyroxenitic mantle with trace element characteristics of EM1 OIB. Much lower Ca and Ca/Fe in the olivines of the northern Payenia than expected for peridotite melts with the given wr compositions is suggested to be due to high magmatic H_2O contents lowering the partition

coefficient for Ca in olivine. Whole-rock Mn/Fe^{2+} shows an excellent correlation with the Mn/Fe ratio in olivine, and therefore the wr compositions of the high Mg# rocks may yield direct information on the mantle lithology from which the melts were derived.

Acknowledgements We are very thankful to Alfons Berger for help with the Electron Microprobe setup and carbon coating. Many thanks go to Mads Alfastsen for discussions and partnership during field work. Also, thanks go to Charlotte Thorup Dyhr and Majken Djurhuus Poulsen for many fruitful discussions. The laboratory work with the ICP-MS analyses by J. Kystol (GEUS) is very much appreciated. We are thankful for the constructive comments by Suzanne M. Kay and an anonymous reviewer. We greatly acknowledge the support to P.M. Holm from the Danish Research Council for Nature and Universe Grant No. 272-07-0514 and the Carlsberg Foundation Grant No. 2010_01_0833 and to N. Søager from the Danish Research Council for Nature and Universe Grant No. 0602-02528B.

References

Beattie P, Ford C, Russell D (1991) Partition coefficients for olivine-melt and orthopyroxene-melt systems. Contrib Miner Petrol 109:212–224

Bertotto GW, Cingolani CA, Bjerg EA (2009) Geochemical variations in Cenozoic backarc basalts at the border of La Pampa and Mendoza provinces, Argentina. J S Am Earth Sci 28:360–373

Cahill TA, Isacks BL (1992) Seismicity and shape of the subducted Nazca plate. J Geophys Res 97(B12):17503–17529. doi:10.1029/92JB00493

Davis FA, Hirschmann MM, Humayun M (2011) The composition of the incipient partial melt of garnet peridotite at 3 GPa and the origin of OIB. Earth Planet Sci Lett 308:380–390. doi:10.1016/j.epsl.2011.06.008

Davis FA, Humayun M, Hirschmann MM, Cooper RS (2013) Experimentally determined mineral/melt partitioning of first-row transition elements (FRTE) during partial melting of peridotite at 3 GPa. Geochim Cosmochim Acta 104:232–260

Dyhr CT, Holm PM, Llabías EJ, Scherstén A (2013a) Subduction controls on Miocene back-arc lavas from Sierra de Huantraico and La Matancilla and new 40Ar/39Ar dating from the Mendoza Region, Argentina. Lithos 179:67–83. doi:10.1016/j.lithos.2013.08.007

Dyhr CT, Holm PM, Llambías EJ (2013b) Geochemical constraints on the relationship between the Miocene-Pliocene volcanism and tectonics in the Mendoza Region, Argentina; new insights from $^{40}Ar/^{39}Ar$ dating, Sr–Nd–Pb isotopes and trace elements. J Volcanol Geotherm Res 266:50–68. doi:10.1016/j.jvolgeores.2013.08.005

Evans KA, Elburg MA, Kamenetsky VS (2012) Oxidation state of subarc mantle. Geology 40:783–786. doi:10.1130/G33037.1

Feig ST, Koepke J, Snow JE (2006) Effect of water on tholeiitic basalt phase equilibria: an experimental study under oxidizing conditions. Contrib Miner Petrol 152:611–638. doi:10.1007/s00410-006-0123-2

Foley SF, Prelevic D, Rehfeldt T, Jacob DE (2013) Minor and trace elements in olivines as probes into early igneous and mantle melting processes. Earth Planet Sci Lett 363:181–191. doi:10.1016/j.epsl.2012.11.025

Folguera A, Naranjo JA, Orihashi Y, Sumino H, Nagao K, Polanco E, Ramos VA (2009) Retroarc volcanism in the northern San Rafael Block (34°–35°30′S), southern Central Andes: occurrence, age and tectonic setting. J Volcanol Geoth Res 186:169–185. doi:10.1016/j.jvolgeores.2009.06.012

Gavrilenko M, Ozerov A, Kyle PR, Carr MJ, Nikulin A, Vidito C, Danyushevsky L (2016) Abrupt transition from fractional crystallization to magma mixing at Gorely volcano (Kamchatka) after caldera collapse. Bull Volcanol 78:47

Grove LT, Chatterjee N, Parman WS, Médard E (2006) The influence of H_2O on mantle wedge melting. Earth Planet Sci Lett 249:74–89. doi:10.1016/j.epsl.2006.06.043

Gudnason J, Holm PM, Søager N, Llambías EJ (2012) Geochronology of the late Pliocene to recent volcanic activity in the Payenia back-arc volcanic province, Mendoza. Argetina J S Am Earth Sci 37:191–201

Herzberg C (2006) Petrology and thermal structure of the Hawaiian plume from Mauna Kea volcano. Nature 444:605–609. doi:10.1038/nature05254

Herzberg C (2011) Identification of source lithology in the Hawaiian and Canary Islands: implications for origins. J Petrol 52:113–146. doi:10.1093/petrology/egq075

Herzberg C, O'Hara MJ (2002) Plume-associated ultramafic magmas of phanerozoic age. J Petrol 43:1857–1883. doi:10.1093/petrology/43.10.1857

Hofmann AW, White WM (1982) Mantle plumes from ancient oceanic crust. Earth Planet Sci Lett 57:421–436

Holm PM, Søager N, Dyhr CT, Nielsen MR (2014) Enrichments of the mantle sources beneath the Southern Volcanic Zone (Andes) by fluids and melts derived from abraded upper continental crust. Contrib Miner Petrol 167:1004. doi:10.1007/s00410-014-1004-8

Holm PM, Søager N, Alfastsen M, Bertotto GW (2016) Subduction zone mantle enrichment by fluids and Zr-depleted crustal melts as indicated by backarc basalts of the Southern Volcanic Zone, Argentina. Lithos 262:135–152. doi:10.1016/j.lithos.2016.06.029

Humayun M, Qin LP, Norman MD (2004) Geochemical evidence for excess iron in the mantle beneath Hawaii. Science 306:91–94. doi:10.1126/science.1101050

Jackson G, Dasgupta R (2008) Compositions of HIMU, EM1, and EM2 from global trends between radiogenic isotopes and major elements in ocean island basalts. Earth Planet Sci Lett 276:175–186. doi:10.1016/j.epsl.2008.09.023

Jackson MG, Hart SR, Koppers AAP, Hubert S (2007) The return of subducted continental crust in Samoan lavas. Nature 448:684–687. doi:10.1038/nature06048

Jacques G, Hoernle K, Gill J, Hauff F, Wehrmann H, Garbe-Schönberg D, van den Bogaard P, Bindeman I, Lara LE (2013) Across-arc geochemical variations in the Southern Volcanic Zone, Chile (34.5°S–38.0°S): constraints on mantle wedge and slab input compositions. Geochem Cosmochem Acta 123:218–243. doi:10.1016/j.gca.2013.05.016

Jochum KP, Nehring F (2006) GeoReM preferred values. Max-Plank-Institut für Chemie, 11/2006. http://georem.mpch-mainz.gwdg.de

Jurewicz AJG, Watson EB (1988) Cations in olivine: 1. Calcium partitioning and calcium-magnesium distribution between olivines and coexisting melts, with Petrologic Applications. Contrib Miner Petrol 99:176–185

Kamenetsky VS, Elburg M, Arculus R, Thomas R (2006) Magmatic origin of low-Ca olivine in subduction-related magmas: co-existence of contrasting magmas. Chem Geol 233:346–357

Kay SM, Copeland P (2006) Early to middle Miocene backarc magmas of the Neuquén basin: geochemical consequences of slab shallowing and the westward drift of South America. In: Kay SM, Ramos VA (eds) Evolution of an andean margin: a tectonic and magmatic view from the andes to the Neuquén Basin (35°S–39°S Lat.). Geol Soc Am Spec Pap 407: 185–213

Kay RW, Kay SM (1993) Delamination and delamination magmatism. Tectonophysics 219:177–189

Kay SM, Mpodozis C (2002) Magmatism as a probe to the Neogene shallowing of the Nazca plate beneath the modern Chilean flatslab. J S Am Earth Sci 15:39–57. doi:10.1016/S0895-9811(02)00005-6

Kay SM, Gorring M, Ramos VA (2004) Magmatic sources, setting, and causes of Eocene to Recent Patagonian plateau magmatism (36°S–52°S latitude). Revista de la Asociación Geológica Argentina 59:556–568

Kay SM, Godoy E, Kurtz A (2005) Episodic arc migration, crustal thickening, subduction erosion, and magmatism in the south-central Andes. Geol Soc Am Bull 117(1–2):67–88

Kay SM, Burns WM, Copeland P, Mancilla O (2006a) Upper Cretaceous to Holocene magmatism and evidence for transient Miocene shallowing of the subduction zone under the northern Neuquén Basin. In Kay SM, Ramos VA (eds) Evolution of an Andean margin: a tectonic and magmatic view from the andes to the Neuquén Basin (35°S–39°S lat.) Geol Soc Am Spec Pap 407: 19–60

Kay SM, Mancilla O, Copeland P (2006b) Evolution of the late Miocene Chachahuén volcanic complex at 37°S over a transient shallow subduction zone under the Neuquén Andes. Evolution of an Andean margin: a tectonic and magmatic view from the Andes to the Neuquén Basin (35°–39°S). Geol Soc Am Spec Pap 407:215–246

Kay SM, Jones HA, Kay RW (2013) Origin of tertiary to recent EM- and subduction-like chemical and isotopic signatures in Auca Mahuida region (37°S–38°S) and other Patagonian plateau lavas. Contrib Miner Petrol 166:165–192. doi:10.1007/s00410-013-0870-9

Kessel R, Schmidt MW, Ulmer P, Pettke T (2005) Trace element signature of subduction-zone fluids, melts and supercritical liquids at 120–180 km depth. Nature 437:724–727. doi:10.1038/nature03971

Kogiso T, Tatsumi Y, Nakano S (1997) Trace element transport during dehydration processes in the subducted oceanic crust: 1. Experiments and implications for the origin of ocean island basalts. Earth Planet Sci Lett 148:193–205. doi:10.1016/S0012-821X(97)00018-6

Laubier M, Grove TL, Langmuir CH (2014) Trace element mineral/melt partitioning for basaltic and basaltic andesitic melts: an experimental and laser ICP-MS study with application to the oxidation state of mantle source regions. Earth Planet Sci Lett 392:265–278

le Roux PJ, le Roex AP, Schilling JG (2002) MORB melting processes beneath the southern Mid-Atlantic Ridge (40°S–55°S): a role for mantle plume-derived pyroxenite. Contrib Miner Petrol 144:206–229

Le Roux V, Lee CTA, Turner SJ (2010) Zn/Fe systematics in mafic and ultramafic systems: implications for detecting major element heterogeneities in the Earth's mantle. Geochim Cosmochim Acta 74:2779–2796. doi:10.1016/j.gca.2010.02.004

le Roux VL, Dasgupta R, Lee C-T (2011) Mineralogical heterogeneities in the Earth's mantle: constraints from Mn Co, Ni and Zn partitioning during partial melting: earth Planet. Sci Lett 307:395–408

Lee C-T, Cheng X, Horodyskyj U (2006) The development and refinement of continental arcs by primary basaltic magmatism, garnet pyroxenite accumulation, basaltic recharge and delamination: insights from the Sierra Nevada, California. Contrib Miner Petrol 151:222–242. doi:10.1007/s00410-005-0056-1

Libourel G (1999) Systematics of calcium partitioning between olivine and silicate melt: implications for melt structure and calcium content of magmatic olivines. Contrib Miner Petrol 136:63–80

Litvak VD, Spagnuolo MG, Folguera A, Poma S, Jones RE, Ramos VA (2015) Late Cenozoic calc-alkaline volcanism over the Payenia shallow subduction zone, South-Central Andean back-arc 34°30′–37°S). Argentina J S Am Earth Sci 64:365–380

Lucassen F, Wiedicke M, Franz G (2010) Complete recycling of a magmatic arc: evidence from chemical and isotopic composition of Quaternary trench sediments in Chile (36°S–40°S). Int J Earth Sci 99:687–701. doi:10.1007/s00531-008-0410-4

McDonough WF, Sun SS (1995) The composition of the Earth. Chem Geol 120(3–4):223–253. doi:10.1016/0009-2541(94)00140-4

Mysen B (2007) Partitioning of calcium, magnesium, and transition metals between olivine and melt governed by the structure of the silicate melt at ambient pressure. Am Miner 92:844–862. doi:10.2138/am.2007.2260

Plank T (2005) Constraints from thorium/lanthanum on sediment recycling at subduction zones and the evolution of the continents. J Petrol 46:921–944. doi:10.1093/petrology/egi005

Portnyagin M, Hoernle K, Plechov P, Mironov N, Khubunaya S (2007) Constraints on mantle melting and composition and nature of slab components in volcanic arcs from volatiles (H_2O, S, Cl, F) and trace elements in melt inclusions from the Kamchatka Arc. Earth Planet Sci Lett 255(1–2):53–69. doi:10.1016/j.epsl.2006.12.005

Quidelleur X, Carlut J, Tchilinguirian P, Germa A, Gillot P-Y (2009) Paleomagnetic directions from mid-latitude sites in the southern hemisphere (Argentina): contribution to time averaged field models. Phys Earth Planet Inter 172:199–209. doi:10.1016/j.pepi.2008.09.012

Ramos VA, Folguera A (2011) Payenia volcanic province in the Southern Andes: an appraisal of an exceptional quaternary tectonic setting. J Volcanol Geotherm Res 201:53–64. doi:10.1016/j.jvolgeores.2010.09.008

Ramos VA, Kay SM (2006) Overview of the tectonic evolution of the southern Central Andes of Mendoza and Neuquén (35°S–39°S latitude). Geol Soc Am Spec Pap 407:1–17

Roeder LP, Emslie FR (1970) Olivine-liquid equilibrium. Contrib Miner Petrol 29:275–289. doi:10.1007/BF00371276

Rudnick RL, Gao S (2003) Composition of the continental crust. In: Carlson RW, Holland HD, Turekian KK (eds) Treatise on geochemistry: the crust. Elsevier, Oxford, pp 1–64

Salters VJM, Stracke A (2004) Composition of the depleted mantle. Geochem Geophys Geosyst 5:5. doi:10.1029/2003GC000597

Scholl DW, von Huene R, Vallier TL, Howell DG (1980) Sedimentary masses and concepts about tectonic processes at underthrust ocean margins. Geology 8:564–568

Søager N, Holm PM (2013) Melt-peridotite reactions in upwelling eclogite bodies: constraints from EM1-type alkaline basalts in Payenia, Argentina. Chem Geol 360–361:204–219. doi:10.1016/j.chemgeo.2013.10.024

Søager N, Holm PM, Llambías EJ (2013) Payenia volcanic province, southern Mendoza, Argentina: OIB mantle upwelling in a back-arc environment. Chem Geol 349–350:36–53. doi:10.1016/j.chemgeo.2013.04.007

Søager N, Holm PM, Thirlwall MF (2015a) Sr, Nd, Pb and Hf isotopic constraints on mantle sources and crustal contaminants in the Payenia volcanic province, Argentina. Lithos 212–215:368–378. doi:10.1016/j.lithos.2014.11.026

Søager N, Portnyagin M, Hoernle K, Holm PM, Hauff F, Garbe-schönberg D (2015b) Olivine major and trace element compositions in Southern Payenia Basalts, Argentina: evidence for pyroxenite-peridotite melt mixing in a back-arc setting. J Petrol 56(8):1495–1518. doi:10.1093/petrology/egv043

Sobolev AV, Hofmann AW, Sobolev SV, Nikogosian IK (2005) An olivine-free mantle source of Hawaiian shield basalts. Nature 434:590–597. doi:10.1038/nature03411

Sobolev AV, Hofmann AW, Kuzmin DV, Yaxley GM, Arndt NT, Chung S-L, Danyushevsky LV, Elliott T, Frey FA, Garcia MO, Gurenko AA, Kamenetsky VS, Kerr AC, Krivolutskaya NA, Matvienkov VV, Nikogosian IK, Rocholl A, Sigurdsson IA,

Sushchevskaya NM, Tekley M (2007) The amount of recycled crust in sources of mantle-derived melts. Science 316:412–417. doi:10.1126/science.1138113

Stern CR (1991) Role of subduction erosion in the generation of the Andean magmas. Geology 19:78–81

Stern CR (2011) Subduction erosion: rates, mechanisms, and its role in arc magmatism and the evolution of the continental crust. Gondwana Res 20:284–308. doi:10.1016/j.gr.2011.03.006

Stracke A, Hofmann AW, Hart SR (2005) FOZO, HIMU, and the rest of the mantle-zoo. Geochem Geophys Geosyst 6:5. doi:10.1029/2004GC000824

Straub SM, LaGatta AB, Martin-Del Pozzo AL, Langmuir CH (2008) Evidence from high-Ni olivines for a hybridized peridotite/pyroxenite source for orogenic andesites the Central Mexican Volcanic Belt. Geochem Geophys Geosyst 9:3. doi:10.1029/2007GC001583

Straub SM, Gomez-Tuena A, Stuart FM, Zellmer GF, Espinasa-Parena R, Cai Y, Lizuka Y (2011) Formation of hybrid arc andesites beneath thick continental crust. Earth Planet Sci Lett 303:337–347. doi:10.1016/j.epsl.2011.01.013

Straub SM, Zellmer GF, Gomez-Tuena AG, Espinasa-Parena R, Pozzo Martin-del, Stuart FM, Langmuir CH (2014) A genetic link between silicic slab components and calc-alkaline arc volcanism in central Mexico. Geol Soc Lond Spec Publ 385:31–64

von Huene R, Scholl DW (1991) Observations at convergent margins concerning sediment subduction, subduction erosion and the growth of continental crust. Rev Geophys 29(3):279–316

Walter MJ (1998) Melting of Garnet peridotite and the origin of Komatiite and depleted lithosphere. J Petrol 39(1):29–60. doi:10.1093/petroj/39.1.29

Wehrmann H, Hoernle K, Jacques G, Garbe-Schönberg D, Schumann K, Mahlke J, Lara LE (2014) Volatile (sulphur and chlorine), major, and trace element geochemistry of mafic to intermediate tephras from the Chilean Southern Volcanic Zone (33°S–43°S). Int J Earth Sci (Geol Rundsch) 103:1945–1962

Willbold M, Stracke A (2006) Trace element composition of mantle end-members: implications for recycling of oceanic and upper and lower continental crust. Geochem Geophys Geosyst 7:4. doi:10.1029/2005GC001005

Workman RK, Hart SR (2005) Major and trace element composition of the depleted MORB mantle (DMM). Earth Planet Sci Lett 231:53–72. doi:10.1016/j.epsl.2004.12.005